

---

[All ETDs from UAB](#)

[UAB Theses & Dissertations](#)

---

2008

## Electroconductive Pet/Swnt Films By Solution Casting

Brian W. Steinert

Follow this and additional works at: <https://digitalcommons.library.uab.edu/etd-collection>

---

### Recommended Citation

Steinert, Brian W., "Electroconductive Pet/Swnt Films By Solution Casting" (2008). *All ETDs from UAB*. 6658.

<https://digitalcommons.library.uab.edu/etd-collection/6658>

This content has been accepted for inclusion by an authorized administrator of the UAB Digital Commons, and is provided as a free open access item. All inquiries regarding this item or the UAB Digital Commons should be directed to the [UAB Libraries Office of Scholarly Communication](#).

ELECTROCONDUCTIVE PET/SWNT FILMS BY SOLUTION CASTING

by

BRIAN W. STEINERT

DERRICK R. DEAN, COMMITTEE CHAIR  
J. BARRY ANDREWS  
ROBIN D. GRIFFIN

A THESIS

Submitted to the graduate faculty of The University of Alabama at Birmingham,  
in partial fulfillment of the requirements for the degree of  
Master of Science

BIRMINGHAM, ALABAMA

2008

# ELECTROCONDUCTIVE PET/SWNT FILMS BY SOLUTION CASTING

BRIAN W. STEINERT

MASTER OF SCIENCE IN MATERIALS ENGINEERING

## ABSTRACT

The market for electrically conductive polymers is rapidly growing, and an emerging pathway for attaining these materials is via polymer-carbon nanotube (CNT) nanocomposites, because of the superior properties of CNTs. Due to their excellent electrical properties and anisotropic magnetic susceptibility, we expect CNTs could be easily aligned to maximize their effectiveness in imparting electrical conductivity to the polymer matrix.

Single-walled carbon nanotubes (SWNT) were dispersed in a polyethylene terephthalate (PET) matrix by solution blending then cast onto a glass substrate to create thin, flexible films. Various SWNT loading concentrations were implemented (0.5, 1.0, and 3.0 wt.%) to study the effect of additive density. The processing method was repeated to produce films in the presence of magnetic fields (3 and 9.4 Tesla).

The SWNTs showed a high susceptibility to the magnetic field and were effectively aligned in the PET matrix. The alignment was characterized with Raman spectroscopy. SWNT and nanocomposite morphology, crystallization behavior, and electrical behavior were also studied. Differential scanning calorimetry (DSC) showed a significant increase in crystallization time and temperature while showing a decrease in crystallinity with increasing concentration of SWNTs. Impedance as a function of frequency was studied to illustrate the effect of SWNT concentration, dispersion, and alignment on electrical properties.

Concentration and dispersion seemed to play very important roles in improving electrical conductivity, while alignment played a secondary and less significant role. The most interesting result proved to be the effect of a magnetic field during processing. It appears that a magnetic field may improve dispersion of unmodified SWNTs, which seems to be more important than alignment. It was concluded that SWNTs offer a good option as conductive, nucleating filler for electroconductive polymer applications, and the utilization of a magnetic field may prove to be a novel method for CNT dispersion that could lead to improved nanocomposite materials.

## DEDICATION

I dedicate this work and accomplishment to the greatest support system I will ever know, my wife, Ashley. You were there every single day, and I've cherished every one of them since we started on this journey together. None of this is possible without you, and there is no way for me to completely express how much I appreciate you, but I know you understand.

*"Honey, you are a rock.....Upon which I stand"*

## ACKNOWLEDGEMENTS

I would like to sincerely express all of my gratitude and appreciation to those people who provided their time, assistance, and overall support during this venture into research and growth. I would first like to acknowledge and thank my advisor, Dr. Derrick R. Dean, for introducing me to my present field of study and paving the way for my future career path. His guidance and advice over the last two years is unmatched, and it is appreciated more than anybody will ever know. I would also like to thank the members of my graduate committee, Dr. Robin D. Griffin and Dr. J. Barry Andrews for all of their input and contributions to this work.

Others that deserve earnest acknowledgement and gratitude include Dr. Jin Gyu Park and Dr. Richard Liang at Florida A&M University, and Dr. Virginia Davis and Vinod Radhakrishnan at Auburn University for their help with Raman spectroscopy. Melissa Chimento at the University of Alabama at Birmingham for her expertise and help in performing transmission electron microscopy. Dr. Arunava Gupta at the University of Alabama for the support in conducting impedance spectroscopy. Dr. Huadong Zeng and Dr. N. Shastry Akella at the University of Alabama at Birmingham for their guidance and support in completing magnetic alignment.

Also, insightful discussion should never be overlooked or underappreciated, which leads me to thank all of my friends and colleagues in the Polymers Lab Group. This is especially true for Keith Green and Mohamed Abdalla who I have used as

trampolines for countless numbers of ideas and questions, taking up countless numbers of hours.

The financial support was provided from NSF (DMR 0404278) grant and the Ireland Tuition Scholarship from the University of Alabama at Birmingham.

Finally, I would also like to acknowledge and thank my family. My mother, Carol, has inspired me with her toughness, determination, and willingness to conquer anything in her path. My siblings, Eric and Shannon, keep me on my toes and motivate me to do better things. My in-laws and extended family, including the Honeycutt's, Campanotta's, Mareno's, and Gagliano's; have shown more love and support than any person could ever ask for, and I don't know how I will ever give back all you have given me. I love you all.

## TABLE OF CONTENTS

	<i>Page</i>
ABSTRACT .....	ii
DEDICATION .....	iv
ACKNOWLEDGEMENTS .....	v
LIST OF TABLES .....	ix
LIST OF FIGURES .....	x
CHAPTER	
1 INTRODUCTION .....	1
2 BACKGROUND .....	4
Carbon Nanotubes .....	4
Synthesis and Growth .....	4
Structure .....	10
Electrical Properties .....	16
Magnetic Properties .....	18
Polymer Nanocomposites .....	20
Processing .....	21
Polymer Matrix .....	23
Electrical Conductivity .....	26
Applications .....	29
3 LITERATURE REVIEW .....	31
Electrical Behavior .....	32
Magnetic Manipulation .....	34
PET Nanocomposites .....	36
4 EXPERIMENTAL .....	37
Materials .....	37
Nanocomposite Film Preparation .....	37

Randomly-oriented Films .....	37
Magnetically Aligned Films .....	39
SWNT Characterization.....	39
Transmission Electron Microscopy (TEM) .....	39
Raman Spectroscopy.....	40
Crystallization Behavior Characterization.....	40
Instrumentation and Setup .....	40
Non-isothermal Crystallization.....	41
Isothermal Crystallization.....	41
Magnetic Alignment Characterization.....	42
Impedance Spectroscopy .....	42
5 RESULTS AND DISCUSSION.....	43
SWNT Morphology .....	43
Crystallization Behavior .....	47
Magnetic Alignment .....	52
Impedance Spectroscopy .....	58
Results.....	59
Analysis.....	62
6 CONCLUSIONS.....	68
LIST OF REFERENCES.....	69

## LIST OF TABLES

<i>Table</i>	<i>Page</i>
1 Structural parameters of a CNT .....	14
2 Summary of experimental choices and electrical conductivity results for polymer-CNT nanocomposites.....	33
3 Non-isothermal crystallization parameters for PET and PET-SWNT composites (n=5), and p-values (ANOVA) with respect to SWNT concentration.....	48
4 Average values for isothermal crystallization times (min.) of PET-SWNT films (n=5), and p-value (ANOVA) for each crystallization temperature with respect to SWNT concentration.....	51

## LIST OF FIGURES

<i>Figure</i>	<i>Page</i>
1 CNT synthesis methods, including (a) arc discharge, (b) laser ablation, (c) chemical vapor deposition, and (d) high-pressure carbon monoxide synthesis.....	7
2 Schematic of tip and root growth of CNTs on a substrate.....	9
3 Bonding behavior of various carbon-based structures, including (a) diamond, (b) graphite, and (c) CNTs.....	12
4 Graphite sheet labeled with multiple integers ( $n, m$ ) and showing the difference in CNT rolling. ....	14
5 Schematic of SWNT and MWNT structures. ....	15
6 Representative density of states of metallic and semi-conducting CNTs.....	17
7 Representative scaled magnetic susceptibility ( $R = \text{CNT radius}$ ) as a function of the applied magnetic field angle, relative to the CNT axis. ....	19
8 Designated recycling nomenclature and chemical structure of PET. ....	24
9 Two separate PET synthesis primary reaction schemes. ....	25
10 Diagram of a composite filler material percolation network. ....	26
11 Film processing flow chart.....	38
12 Digital image of solution cast PET films of varying SWNT loadings (a) 0.0 wt.% SWNT, (b) 0.5 wt.% SWNT, and (c) 1.0 wt.% SWNT. ....	38
13 Diagrams of a representative MRI scanner showing the arrangement of the superconducting magnets and specimen placement. ....	39
14 TEM micrographs of pristine SWNTs showing (a) high aspect ratios, <i>Inset</i> . Isolated SWNTs with small dimensions ( $d \sim 1\text{-}4 \text{ nm}$ ), and (b) bundling.....	43

15 Raman spectra of SWNTs with varying laser excitation wavelengths (488 and 785 nm). <i>Insets.</i> RBM regions with labeled frequency peaks. ....	45
16 Raman spectra of SWNTs sonicated for varying time periods (0-6 hours). <i>Inset.</i> D-peaks of each spectrum between 1200 and 1400 $\text{cm}^{-1}$ .....	46
17 DSC scans of heat flow vs. temperature during non-isothermal crystallization of various PET-SWNT composites at a cooling rate of 10 $^{\circ}\text{C}/\text{min}$ . ....	47
18 DSC scans of heat flow vs. time during isothermal crystallization of various PET-SWNT composites at different crystallization temperatures.....	50
19 Diagrams showing unaligned/aligned CNT response to an excitation laser and sample orientation notation relative to an applied magnetic field during processing.....	52
20 G-peak spectra of an unaligned PET-SWNT nanocomposite film showing the independence of the measurement angle relative to the orientation of the SWNTs. ....	53
21 G-peak intensities relative to the magnetic field direction (0 degrees = parallel) of Raman spectra for samples with varying SWNT loadings and magnetic field processing parameters.....	54
22 TEM micrographs showing the effect of magnetic field strength at a constant SWNT loading (3.0 wt.%). ....	56
23 Log-log plot of the AC conductivity as a function of frequency for various nanocomposite samples. ....	60
24 Log(AC conductivity) as a function of SWNT mass fraction showing dependence on magnetic field strength, and the relative applications based on the values. ....	61

## CHAPTER 1

### INTRODUCTION

From ancient straw and mud bricks for shelter to contemporary reinforced carbon-carbon tiles for the space shuttle, composites have managed to engineer a long and notable history in the world of materials. Defined as a material system with two or more constituents, a composite can be applied to numerous industry needs and circumstances due to the superior property ranges that can be produced from multiple components. A relatively newer class of composites, called ‘nanocomposites’, due to one constituent of the material possessing a nanoscale ( $10^{-9}$  m) dimension, is quickly gaining interest and momentum in a variety of diverse fields. Structural protection and support, barrier and thermal management, and electronics are all areas which will potentially benefit from the utilization of nanocomposites. They offer an advantage because the nanoscale component transfers its properties to the matrix much more efficiently than normal composites, due to a much greater surface area to volume ratio that results in more matrix-filler interaction.

Nanocomposites come in several forms, with the most common types combining a polymer matrix with a clay or carbon-based nanoscale filler. Carbon-based fillers, such as carbon nanotubes (CNTs) and carbon nanofibers (CNFs), are of particular interest with respect to electronic applications, because they have been shown to conduct electricity very efficiently [1-9]. By producing a polymer nanocomposite with conducting filler,

one can potentially create a tougher, lighter, and cheaper material for various electrical applications.

In a report published by Business Communications Company, Inc., the total North American market for electroactive/conductive polymers reached 128.5 million pounds valued at \$205.3 million in 2003 [10]. These numbers are estimated to rise to 745 million pounds at a value of almost \$1.6 billion by 2008, representing a growth of 9.8% in total volume per year and 15.3% in value per year [10]. This information strongly expresses the value of research in this area.

Electroconductive polymers, generally thermoplastics, are commonly described as pure polymer conductive plastics (e.g. polypyrrole, polythiophene, and polyaniline) or composites which require the addition of conductive fillers. The areas that encompass this market include antistatic applications, electrostatic dissipation, battery technology, flexible electronics, and electromagnetic shielding. Electromagnetic interference (EMI) shielding is crucial in numerous electronic devices, and presently metal is used most often for this application. An electroconductive polymer would significantly reduce weight, manufacturing cost, and provide a much better surface finish [11]. CNTs offer great potential in this vast expanding market, because of their nanoscale dimensions, fiber-like geometry, and excellent electrical properties.

Though the promise of innovative CNT nanocomposites exists, many issues still need to be solved before they can reach their technological potential. The goal of the research presented in this manuscript is to investigate relationships between processing, structure, and electrical properties of a novel electroconductive polymer composite with the addition of CNTs.

The objectives of this research were investigated through the production of solution cast nanocomposite thin films. Unmodified single-walled CNTs (SWNTs) and polyethylene terephthalate (PET) were chosen as the filler and matrix materials, respectively. Magnetic fields were employed to establish anisotropy into the system via SWNT alignment. The effects of the materials and processing parameters were examined by measuring crystallization behavior, degree of alignment, and the electrical properties.

## CHAPTER 2

### BACKGROUND

#### Carbon Nanotubes

CNTs have come to the forefront of nanostructured materials research in the past decade. Interest has grown exponentially since the official discovery and characterization of CNTs in 1991 [12], with only 9 papers or books containing the words ‘carbon nanotubes’ published in 1992 and more than 6,500 in 2006. This incredible growth and excitement over CNT research is almost solely due to their excellent, inherent properties and their wide realm of potential applications. These properties include outstanding tensile strength and modulus, high thermal conductivity, chemical reactivity as well as resistance, and potentially selective electrical properties. These attributes, along with their nanoscale dimension and high aspect ratios (length/diameter), make them extremely attractive as reinforcement filler in nanocomposite materials, scanning probes, energy storage, sensors, and a multitude of electronic devices.

#### *Synthesis and Growth*

CNT utilization begins with production and cost. Economics dictates that there be a need and demand for a particular product to thrive. In order to create and increase that demand, one must get significant return on an investment. For CNTs, the applications are extremely prevalent and the research is growing. Therefore, the

production and synthesis of CNTs is vital for growth, and it may be one of the few minor barriers inhibiting CNT potential in the marketplace. Creating cheap and reliable CNT production mechanisms is a cornerstone of research.

There are a few basic requirements when attempting to manufacture CNTs, which include an active catalyst, a source of carbon, and sufficient energy to carry out the synthesis and growth mechanisms. Several different methods are frequently employed to fulfill these requirements.

The first is the arc discharge method (Figure 1a). Arc discharge involves using a power supply to create an electric arc across a small gap between two graphite electrodes (with or without a catalyst) under an inert atmosphere and at pressures between 100 and 1000 torr. Both forms of CNTs, multi-walled carbon nanotubes (MWNTs) and SWNTs, can be produced with this method. CNT diameters can be controlled by adjusting the inert gas composition, and the yield can be controlled by the overall gas pressure. This method is relatively easy and cheap. However, the CNTs produced with this method require extensive purification to use them effectively [13, 14].

A second method for producing CNTs is known as laser ablation (vaporization) (Figure 1b). This method involves evaporating a graphite target (with or without a catalyst) with a pulsed or continuous laser beam under an inert atmosphere. This method produces unwanted by-products along with CNTs and both are gathered onto a cold collector. It is very similar to arc discharge and in both cases metal catalysts are required to produce SWNTs, while MWNTs are formed in the absence of a catalyst [13, 14].

While arc discharge and laser ablation methods are considered ‘plasma-based’ methods, there are other techniques that are ‘thermal-based’ methods for producing

CNTs. The first of these thermal methods is chemical vapor deposition (CVD) (Figure 1c). CVD involves forcing gaseous carbon to flow over transition metal catalyst nanoparticles on a substrate at escalated temperatures (550 to 1200 °C). It has been shown to produce high-bulk quantities at very high purities (99% with no amorphous carbon). Due to this, CVD seems to offer great potential for producing high quality, affordable CNTs for industry needs and applications [13, 14].

Another method closely related to CVD is high-pressure carbon monoxide synthesis (HiPco) (Figure 1d). It involves injecting a metal catalyst precursor along with gaseous carbon monoxide (CO) into a reactor. CNTs are formed by the disproportionation of CO by the nanometer-size catalyst. HiPco is very promising in industry due to the high quantity (up to kilograms), high quality (97% atomic purity), and narrow diameter distributions (between 0.7 and 1.1 nm) that is normally seen in the final product. The CNT diameter range can be controlled by varying the pressure inside the reactor, and the catalyst composition [13, 14].

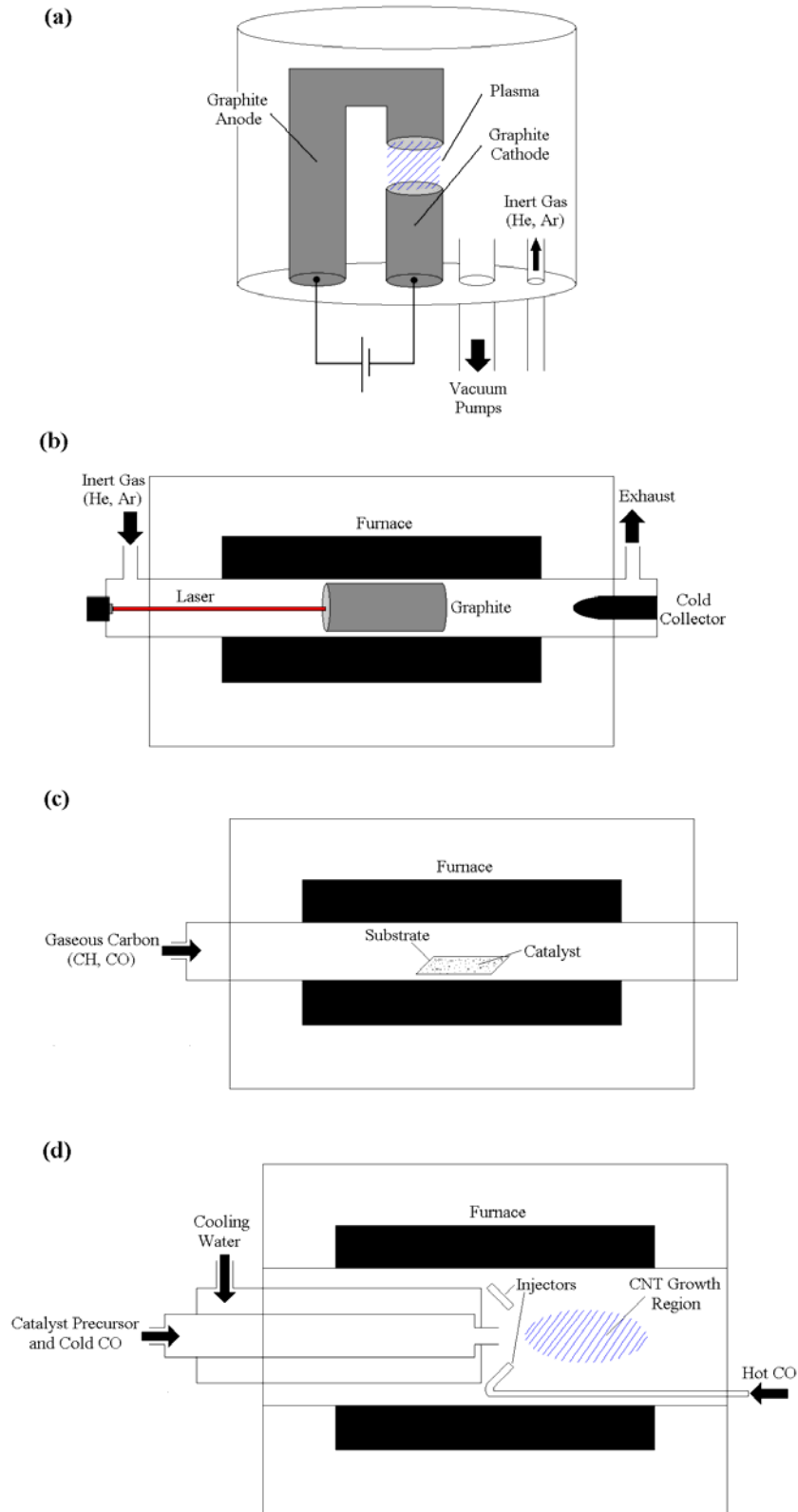


Figure 1. CNT synthesis methods, including (a) arc discharge, (b) laser ablation, (c) chemical vapor deposition, and (d) high-pressure carbon monoxide synthesis.

Since CVD, and the analogous HiPco process, offer the greatest potential for large-scale production, the variables and resultant growth behavior of this type of method should be scrutinized closely. To begin, deposition growth is directly associated with the location of the catalyst particle, and it can be split into two distinct categories: gas phase growth and substrate growth. In gas phase growth, the catalyst particle and subsequent CNT growth are found in suspension. In substrate growth, the catalyst is found on a specific surface with the ensuing CNT growth occurring perpendicular and away from it to create a vertical ‘forest’ of CNTs. The CNTs grow and remain upright because of the van der Waals forces that exist between the outermost walls of a CNT, and its neighbors, which produce bundling of the CNTs [15].

Both methods of growth will essentially follow a similar growth mechanism, which can be broken down into the following steps:

1. Diffusion or movement of precursor catalyst to a substrate or area in space.
2. Adsorption of reactive species/feedstock onto the particle surface.
3. Reactions on the particle surface causing CNT and by-product formation.
4. Desorption of by-product away from the particle surface.

The resulting CNT product parameters (e.g. quantity, purity, size, and chirality), are highly dependent upon numerous variables that effect these steps, including catalyst size and composition, reactor temperature and pressure, substrate and carbon feedstock composition, and injection rates. The wide range of variables and uncertainty in the process makes CNT growth very difficult to decipher and understand. However, two common models are typically referenced with respect to CNT growth: root (base) growth and tip growth (Figure 2) [13-15].

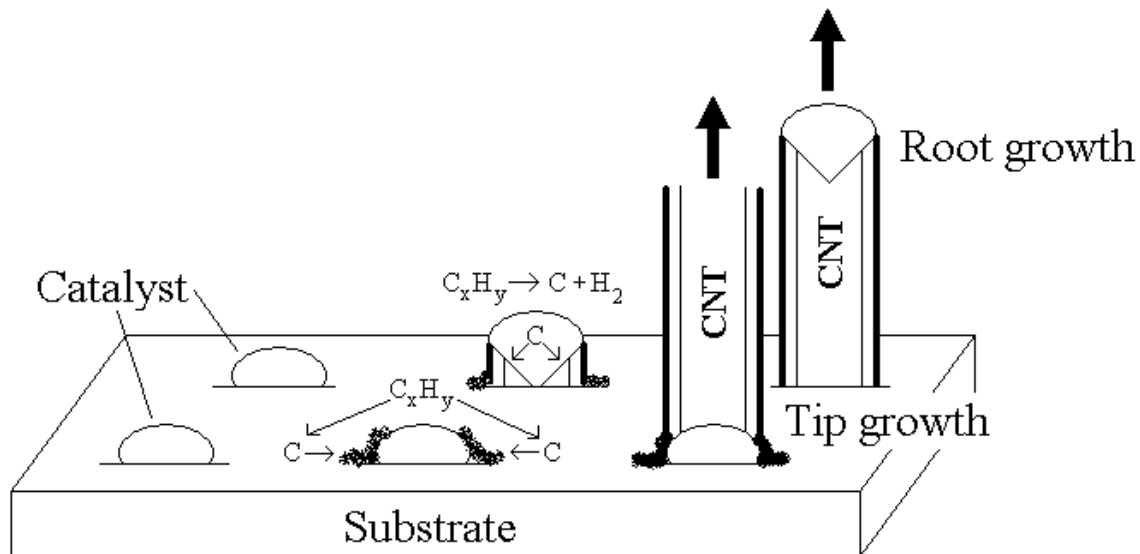


Figure 2. Schematic of tip and root growth of CNTs on a substrate.

In either case, a hydrocarbon from the carbon feedstock adsorbed on a catalyst surface decomposes and releases carbon. The carbon then diffuses into the catalyst particle or around its surface until a saturation point is reached. Once carbon is supersaturated, it precipitates in a crystalline tubular structure. At this point root or tip growth will ensue, and the dominant variable in determining the chosen route of growth is the strength of the catalyst-substrate interaction. If the particle is strongly adhered to the substrate, then carbon will precipitate upward from the particle surface (tip growth). If there is weak adherence, then carbon precipitates at the bottom of the particle and lifts it away from the substrate as growth occurs (root growth). It is believed that tip growth is the principal mechanism for MWNT formation, while root growth is the principal mechanism for SWNT formation [13].

The growth interruption mechanism is dependent on several variables. First, it is vital that there is a constant supply of carbon diffusing through the catalyst particle. An interruption in the feedstock flow or a build up of amorphous carbon around the particle

surface to create a ‘shell’ can disrupt the process and halt growth. Also, any substantial external forces that can oppose the growth mechanisms may result in early growth interruption [13].

### *Structure*

Carbon is an extremely versatile and prevalent particle, and carbon-based structures arise in a variety of allotropes, including diamond, graphite, buckminsterfullerenes (‘bucky balls’), and CNTs. These various arrangements occur because of several different bonding behaviors that carbon can undergo. A carbon atom has six electrons, with the two innermost electrons being strongly bonded and filling the 1s orbital. The four outermost electrons, or valence electrons, are weakly bonded and fill 2s<sup>2</sup> and 2p<sup>2</sup> orbital. Due to the small energy difference between the upper 2p and lower 2s energy levels, these valence electrons can mix with each other and go through a process called hybridization. There are three possible hybridizations of carbon, which include sp, sp<sup>2</sup>, and sp<sup>3</sup>. These hybridizations determine the carbon-based molecule configuration and ultimately the physical properties of the material.

In diamond, sp<sup>3</sup> hybridization occurs and produces four equal σ covalent bonds in a tetrahedral configuration (Figure 3a). The strong bonding and tight, interlocking structure imparts extreme properties to diamond, including tremendous hardness and high electrical resistance.

In graphite, planar sp<sup>2</sup> hybridization occurs for three of the four valence electrons to form three in-plane σ covalent bonds while the fourth electron forms a much weaker out-of-plane π bond (Figure 3b). Actually, the σ bond in sp<sup>2</sup> hybridization is stronger

than a  $\sigma$  bond in  $sp^3$  hybridization, which means graphite is stronger than diamond in-plane. However, the weaker interaction of the  $\pi$  bond between the hexagonal planes allows them to slide quite readily between themselves, which makes graphite a relatively soft material. This 'loose'  $\pi$  electron also enhances the electrical conductivity of graphite compared to diamond.

CNTs basically experience  $sp^2$  hybridization, because it is essentially a graphite sheet rolled up into a tubular configuration. This rolling of graphite partially deforms the  $sp^2$  hybridization to produce some  $\sigma$ - $\pi$  mixing, or rehybridization of  $sp^2$  to  $sp^3$ . This causes the three  $\sigma$  covalent bonds to be slightly out-of-plane (Figure 3c). At the same time, the curvature of the tube causes quantum confinement and a more delocalized  $\pi$  electron around the tube surface, which produces some very intriguing electrical properties. These bonding characteristics help to produce an assembly that is considerably stronger, more conductive, and more chemically reactive than the simple graphite sheet.

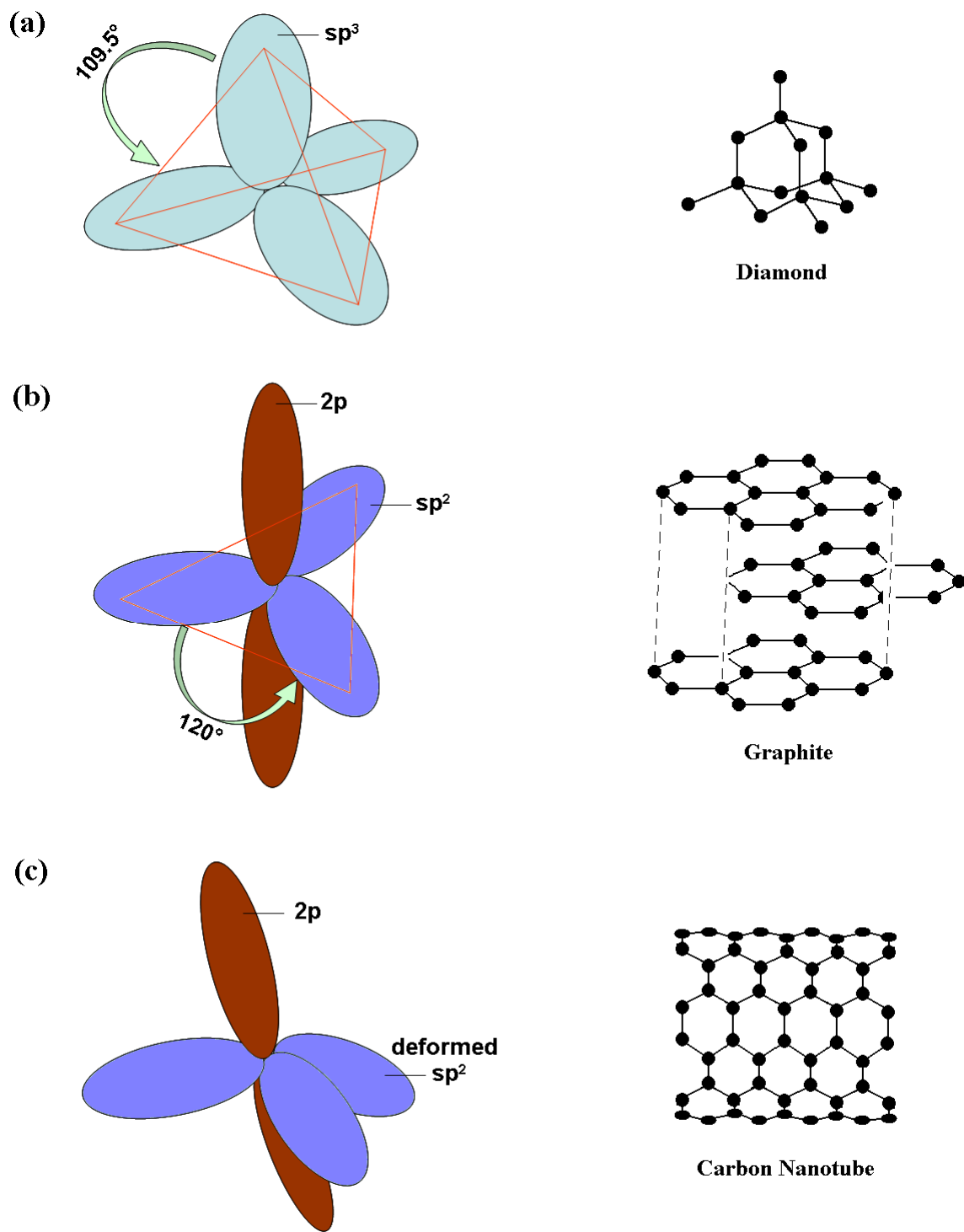


Figure 3. Bonding behavior of various carbon-based structures, including (a) diamond, (b) graphite, and (c) CNTs.

The CNT structure is a simple one, which has been studied extensively by transmission electron microscopy (TEM), atomic force microscopy (AFM), scanning tunneling microscopy (STM), and Raman spectroscopy. It is a one-dimensional (1D) tube with a hexagonal lattice structure and a diameter approximately 1 nm in many cases. Along with the  $sp^2$ /partial  $sp^3$  hybridization and 1D nature, the type of ‘rolling’ a CNT experiences equally helps determine the fundamental properties of the structure. The ‘rolling’ of a CNT can be characterized in terms of the nanotube chirality.

Chirality is defined by the chiral vector ( $\vec{C}_h$ ) and chiral angle ( $\theta$ ). The chiral vector identifies the circumference of the nanotube surface, and the chiral angle defines the degree of rolling of a CNT. The chiral vector and angle can be summarized with a set of vectors ( $n, m$ ), which are used to identify CNTs. Both parameters can be used to differentiate the nanotubes into three distinct groups. These groups are labeled armchair ( $n = m, \theta=30^\circ$ ), zig-zag ( $n > 0, m = 0, \theta=0^\circ$ ), and chiral ( $n > m > 0, 0 < \theta < 30^\circ$ ) (Figure 4) [16]. Each type produces slightly different properties. This is especially true when observing the electrical behavior of CNTs. Table 1 presents various structural parameters for CNTs.

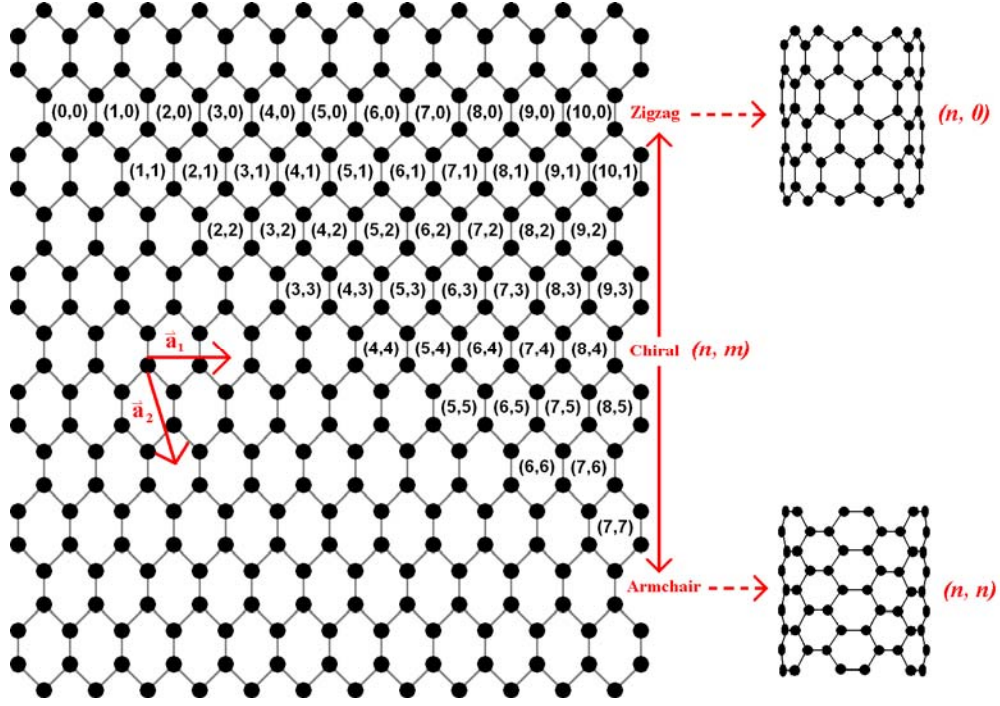


Figure 4. Graphite sheet labeled with multiple integers  $(n, m)$  and showing the difference in CNT rolling.

Table 1. Structural parameters of a CNT.

Symbol	Name	Formula	Value
$a_{c-c}$	carbon-carbon distance		1.421 Å
$a$	length of unit vector	$\sqrt{3}a_{c-c}$	2.46 Å
$\bar{a}_1, \bar{a}_2$	unit vectors	$\left(\frac{\sqrt{3}}{2}, \frac{1}{2}\right)a, \left(\frac{\sqrt{3}}{2}, -\frac{1}{2}\right)a$	in $(x,y)$ coordinates
$\bar{C}_h$	chiral vector	$\bar{C}_h = n\bar{a}_1 + m\bar{a}_2 = (n, m)$	$n, m$ : integers
$L$	circumference of CNT	$L =  \bar{C}_h  = a\sqrt{n^2 + m^2 + nm}$	$0 \leq  m  \leq n$
$d_t$	diameter of CNT	$d_t = \frac{L}{\pi} = \frac{\sqrt{n^2 + m^2 + nm}}{\pi} a$	
$\theta$	chiral angle	$\sin \theta = \frac{\sqrt{3}m}{\sqrt{n^2 + m^2 + nm}}$ $\cos \theta = \frac{2n + m}{2\sqrt{n^2 + m^2 + nm}}$ $\tan \theta = \frac{\sqrt{3}m}{2n + m}$	$0 \leq  \theta  \leq 30^\circ$

The ideal CNT has high structural perfection with low defect density and little to no amorphous carbon. However, there are variations within this carbon allotrope category. The two most common variants, which are dependent upon the synthesis mechanism, are SWNTs and MWNTs. While both have the same basic tubular structure, one may think of the SWNT as the fundamental structural unit and consisting of a single tube, one atom thick all the way around. MWNTs, on the other hand, consist of multiple, diameter-increasing tubes concentrically located around a common axis (Figure 5). The isolated nature of the SWNT makes them stronger than MWNTs due to the fact that the concentric cylinders of the MWNTs tend to slip between each other because of weaker van der Waals forces that hold them together. It also makes SWNTs a much better option for electronic/conductive applications, because the multiple cylinders of a MWNT can interfere with each other as electrons flow along the axis.

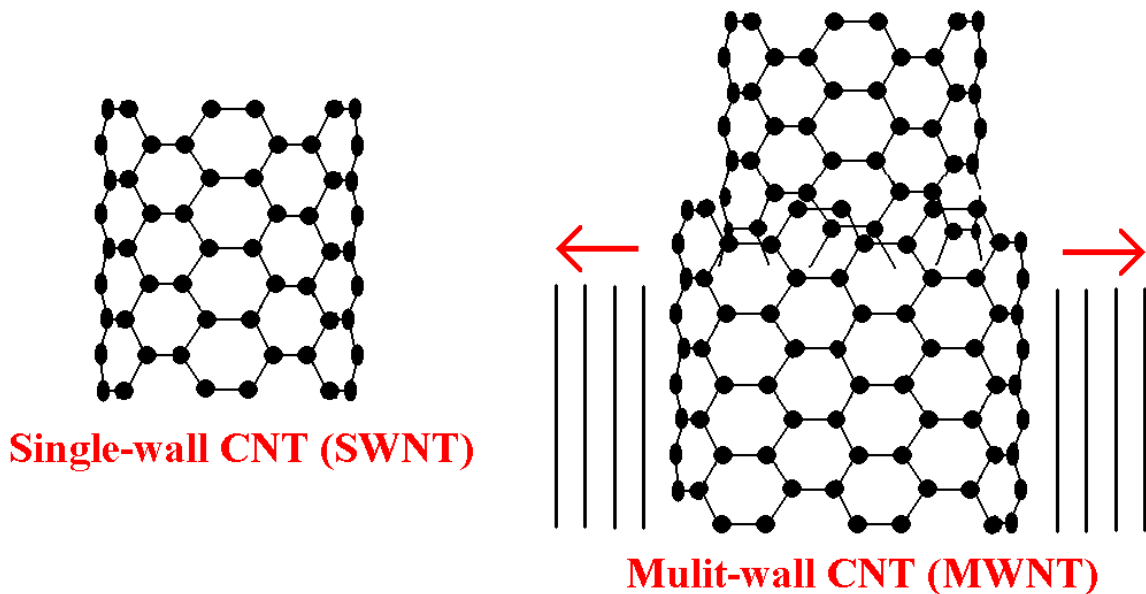


Figure 5. Schematic of SWNT and MWNT structures.

### *Electrical Properties*

The electrical behavior of CNTs is one of the most highly studied areas in all of CNT research due to the potential results in a wide range of applications. Theoretical calculations have shown that the electrical properties of CNTs are very dependent upon their structure, or their rolled configuration (i.e. armchair, zig-zag, or chiral) and diameter more specifically [2, 6]. The nanoscale dimensions, 1D structure, and tubular symmetry produce amazing quantum transport effects. Studies have shown that individual CNTs can behave electrically as a single molecule and be defined as quantum wires [5, 17] with very high conductive capability (resistivity,  $R = 10^{-8} \Omega\text{-cm}$ ) being reported [1, 3, 18]. This is greater than iron or copper ( $R = 10^{-6} \Omega\text{-cm}$ ) [19], as well as crystalline graphite ( $R = 10^{-5} \Omega\text{-cm}$ ) [20].

The origin of CNT electrical properties begin with graphene sheets, which is a single plane of graphite. The electrical behavior of graphene can be determined from their energy dispersion. For single planes of graphene, the conduction and valence bands touch at six points (each hexagonal lattice corner) of the 1<sup>st</sup> Brillouin zone at the Fermi energy, and the energy bands become cone-shaped at these points. These band intersections at the corners mean the charge carriers display linear energy dispersion in the vicinity of these points. This is a very interesting characteristic, and it leads to graphite acting as a semi-metal [21].

As mentioned, the chirality also plays an important role in determining the electrical properties of CNTs, especially SWNTs. Armchair nanotubes ( $n = m$ ) are metallic, while chiral ( $n > m > 0$ ) and zig-zag ( $n > 0, m = 0$ ) may be semi-metallic (small band gap semiconductor) if  $(n - m) = 3i$ , or semi-conducting (large band gap

semiconductor) for all other cases [13]. This unique behavior is due to the quantum confinement mentioned previously and seen in the different electronic band structures that arise from each type of CNT, which is found by imposing periodic boundary conditions around the perimeter of the CNT due to the curvature of the tube. The confinement around the edge of a CNT means the electrons can only move along the axis. This is why CNTs are referred to as quantum wires. The 1D quantum conduction can be seen in a CNTs density of states (DOS) in the form of van Hove singularities (Figure 6). This signature is not seen in a normal graphene plane [22].

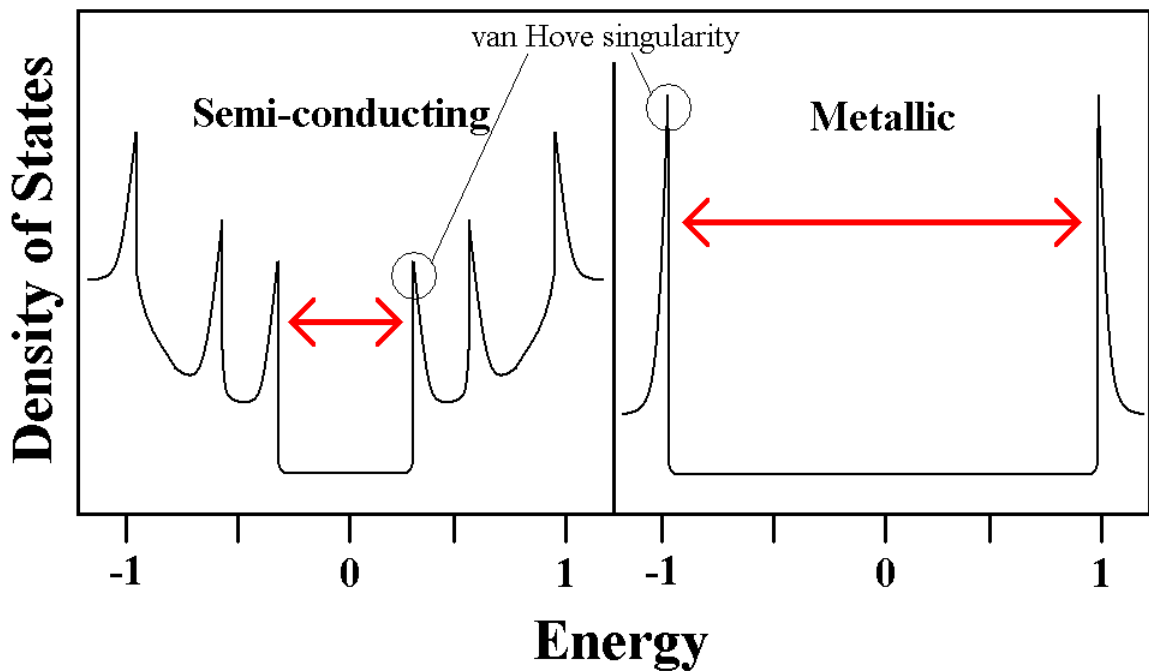


Figure 6. Representative density of states of metallic and semi-conducting CNTs.

Semi-conducting CNTs have been shown to be extremely useful in electronic devices, such as transistors, because of their strong dependence on gate voltage. Durkop et al. reported the highest room temperature field-effect mobility ( $79,000 \pm 8,000$

cm<sup>2</sup>/Vs) and intrinsic mobility (120,000 cm<sup>2</sup>/Vs) ever seen in a semi-conducting device, and they also concluded that the conductivity of semi-conducting nanotubes may be ‘tuned’ from insulating to highly metallic at large enough gate voltages [7]. These attributes make CNTs very attractive in electronic applications.

### *Magnetic Properties*

There is an indelible connection between the electrical and magnetic properties of CNTs. One very interesting and unique characteristic of CNTs is how external magnetic fields affect the electrical behavior of specific types of nanotubes. It has been shown that CNTs can undergo an electrical transition in the presence of a magnetic field applied parallel to the nanotube axis [23-25]. Metallic CNTs can change to semi-conducting, and vice-versa, due to a magnetic field creating an oscillatory shift in their band gaps. This is caused by the phase shift that occurs in the wavefunction along the perimeter of the CNT due to the Aharonov-Bohm effect [24, 25], which is essentially a quantum mechanical effect that occurs along a conducting wire parallel to a magnetic field and causes fluctuations in conductance by diverting electrons.

CNTs have also been shown to be magnetically susceptible [23-29]. Magnetic susceptibility ( $\chi$ ) is the degree of magnetization of a material in response to an applied magnetic field, and it has been the subject of multiple theoretical predictions with respect to CNTs [23, 29]. It was found that  $\chi$  has an increasing, linear dependence on CNT diameter. Also, it has been determined that the  $\chi$  is dependent on magnetic field direction and temperature. Due to magnetic anisotropy, CNTs are able to align in the presence of a magnetic field. If the magnetic field is parallel to the CNT axis, then the magnetic

susceptibility ( $\chi_{||}$ ) for metallic nanotubes is strongly positive (paramagnetic). If the field is perpendicular to the axis, then the susceptibility ( $\chi_{\perp}$ ) is negative (diamagnetic). For semi-conducting nanotubes, both  $\chi_{||}$  and  $\chi_{\perp}$  are negative (diamagnetic) and  $|\chi_{\perp}| > |\chi_{||}|$ . This anisotropic  $\chi$  is the reason magnetic fields may be used for CNT alignment (Figure 7). With respect to temperature,  $\chi_{||}$  decreases for metallic and increases for semi-conducting CNTs as temperature increases, while  $\chi_{\perp}$  increases for both metallic and semi-conducting CNTs as temperature increases [29].

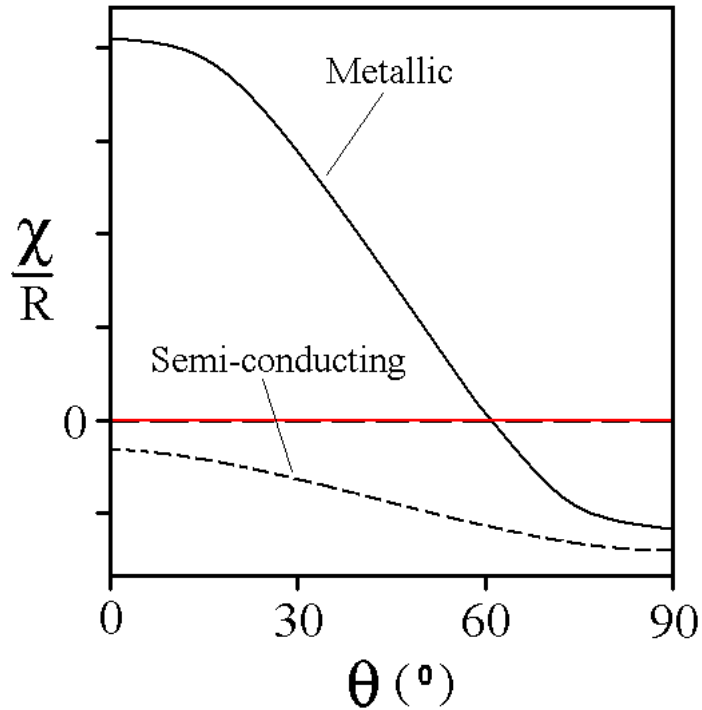


Figure 7. Representative scaled magnetic susceptibility ( $R = \text{CNT radius}$ ) as a function of the applied magnetic field angle, relative to the CNT axis.

## Polymer Nanocomposites

Using CNTs as property enhancing nanofillers for a high performance, lightweight composite is one of the lynchpins of nanocomposite research. These composites have endless applications in numerous industries throughout the world today, including automotive, aerospace, biomedical, and electronics industries. However, the key to utilizing and fulfilling the potential of CNT-based polymer nanocomposites is to research and develop the tools necessary to exploit them, including synthesis mechanisms, processing procedures, characterization techniques, and theory that describes and explains specific behaviors.

There are three major characteristics that define the effectiveness and performance of polymer nanocomposites [30]:

1. Nano-confined matrix polymer

The nanoscale dimension and geometry of a CNT results in a very large interfacial reaction and enable a considerable effect upon the surrounding polymer. The enhanced interface limits polymer chain conformation, and the free energy of polymer near an interface is vitally different than that in the bulk material. Therefore, at relatively low concentrations CNTs can effectively confine the polymer matrix which alters mobility, relaxation behavior, chain ordering and packing, and the resultant crystallite nucleation and growth.

2. Nanoscale constituents (e.g. CNTs, clay silicates)

When the dimensions of a nanoscale constituent approach the fundamental length scale of a physical property, it results in the emergence of new superior properties not normally present in the bulk material. Quantum confinement and paramagnetic response in CNTs

are two previously mentioned examples of this behavior. Dispersing the nanoscale material in the bulk material gives rise to a new material dominated by solid-state physics of the nanoscale component.

### 3. Nanoscale arrangement of the constituents

Extreme system variations can be generated from modifying the spatial arrangements and orientations of the nanoscale constituent within a matrix. Also, closely related to this concept are the constituent interactions between individual particles that establish the degree of distribution (e.g. clustering, heterogeneous dispersion).

In the grand scheme of polymer nanocomposites, it is inaccurate and incomplete to simply report CNT concentration and the polymer matrix material. There are many more important factors contributing to the properties of a nanocomposite, including CNT synthesis and purification processes, CNT aspect ratios, amount and type of CNT impurities, CNT orientation, and nanocomposite/polymer synthesis processes [30]. Though it is difficult to determine some of these experimental factors, being able to more readily answer these questions could improve results and reduce inconsistencies seen in the research.

### *Processing*

There are several different processing methods that are all relatively common for producing thermoplastic and thermoset nanocomposites. These methods include several types of melt processing, solution processing, and in-situ polymerization. Though each technique is fundamentally different, they all attempt to resolve specific concerns for

creating an effective polymer nanocomposite; which include deaggregation, dispersion, interfacial interaction, and alignment in specific instances.

Often it is vital to perform preprocessing of nanoparticles, specifically CNTs, to properly prepare them for incorporation into the polymer. The preprocessing procedure begins by purifying the CNTs to eliminate amorphous carbon, metal catalysts, and any other unwanted by-products. This is commonly done through thermal annealing and acid treatment. Purification is followed by deaggregation of the CNT bundles to enhance dispersion in the matrix. Ultrasonication of the CNTs in a solution is most often used for this purpose. The last step in the preprocessing procedure is chemical functionalization of the CNT surface. This step is much more optional than the previous two steps, but it has been shown to greatly enhance dispersion and interfacial interaction [31, 32].

Once the CNTs have been sufficiently prepared, processing of the nanocomposite can begin. Melt processing is one very popular option. There are various melt processing techniques, including injection molding, blow molding, and extrusion. These techniques are beneficial because they are quick, relatively cheap, and absent of harsh solvents and impurities; which makes them readily available in industry. One of the most effective methods for disrupting and dispersing CNT bundles for melt processed composites is high shear mixing, because it is a high energy method that is able to overcome high melt viscosities while maintaining CNT integrity. High shear mixing not only disperses CNTs, but it also may result in some partial alignment of the CNTs due to the unidirectional forces being concentrated on the melt. Injection molding and spinning extruded fibers have also been shown to effectively align CNTs in a polymer matrix [32, 33].

In-situ polymerization is another processing option. This method does a good job of assimilating the phases of the composite, as well as dispersing the nanofiller. The curing behavior of a thermoset or ultraviolet-curable polymer with dispersed CNTs are examples of this type of processing [32, 33].

The last processing technique that will be discussed is solution processing. Solution processing is advantageous because the low viscosity solutions facilitate CNT dispersion. Solution casting and spin casting/coating are two common solution processing techniques. Both techniques involve pouring a solution onto a substrate and allowing the solvent to evaporate away from the bulk material. Alignment can also be relatively controlled through this process by shearing the solution or stretching the material post process. Another solution-based technique is electrostatic spinning. This technique utilizes an electric potential between two points (solution extrusion point and collecting point) to produce nanoscale composite fibers that will contain aligned CNTs [32, 33].

### *Polymer Matrix*

A specific matrix material for a composite is usually chosen because it is already useful in one or more applications, but it may be deficient in specific qualities. If these ‘deficient qualities’ are improved upon and enabled, then the matrix function for those applications could be greatly improved. By creating a composite, one attempts to improve the material while still maintaining the existing, attractive attributes of the matrix. Some of the most common matrix materials are thermoset and thermoplastic polymers. Epoxies, polyesters, and phenolics are very common thermoset materials.

Common thermoplastics include polyimides, polysulfones, and polyesters. Thermoplastics are attractive because of their superior toughness, flexibility, and optical properties. However, they often exhibit relatively poor thermal stability, electrical conductivity, and mechanical strength. These are the areas where CNTs express their potential as a nanoscale filler material.

The matrix has several important roles in a composite, which include maintaining the desired filler spacing, transmitting loads between fiber layers, and reducing the propensity for stress concentrations to be transmitted from damaged to healthy filler material [34].

One highly regarded commercial polymer is PET. PET is a thermoplastic polyester (Figure 8) with an extremely long and productive history. It is extensively used for numerous applications, including as fibers, films, bottle moldings, and medical supplies to name a few. Its thermal stability associated with a relatively high melting temperature (261-264°C), strong wear and chemical resistance, and low permeability makes it extremely attractive for all of these applications. However, these properties also make it fairly difficult to work with by extending production time, and so it would be advantageous to reduce this setback with respect to crystallization rate and behavior.

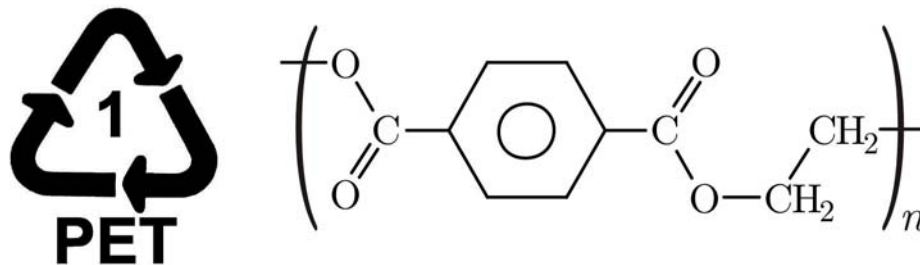
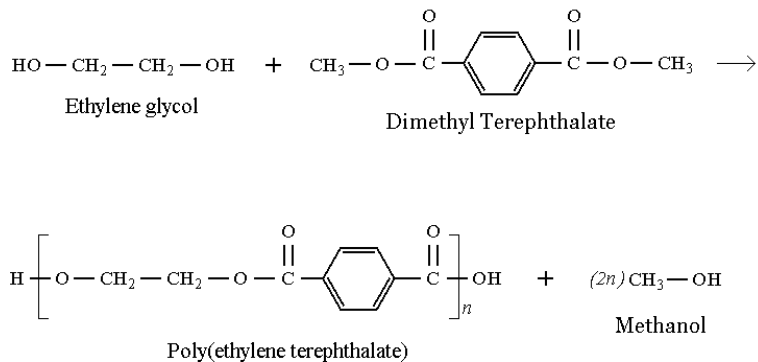


Figure 8. Designated recycling nomenclature and chemical structure of PET.

The procedure for synthesizing PET is referred to as a polyester condensation reaction. PET is commonly produced from ethylene glycol (EG) (alcohol) and either dimethyl terephthalate (DMT) (ester) or terephthalic acid (TPA) (Figure 9). The DMT route is an older method that has predominantly been replaced by the TPA route for PET production. Both processes produce bis-(2-hydroxyethyl)terephthalate (BHET) as an intermediate product. BHET is then polymerized under heat and pressure to produce PET. In the DMT route, transesterification occurs and the main by-product is methanol, while the TPA route creates water. The water by-product is what makes the TPA route favorable for large-scale manufacturing [35].

#### DMT Process



#### TPA Process

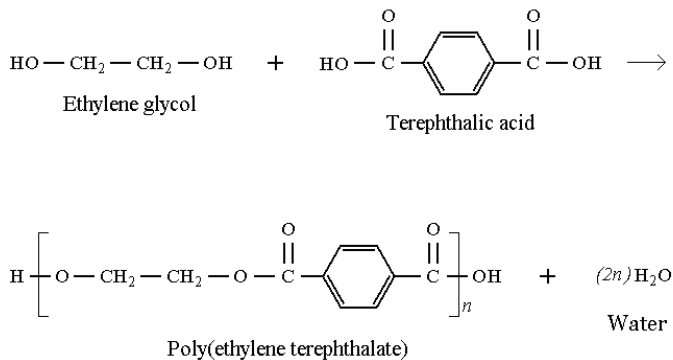


Figure 9. Two separate PET synthesis primary reaction schemes.

### *Electrical Conductivity*

As mentioned, there is a huge market for conductive or electroactive polymers [10], and there has been plenty of research done in this area, especially with respect to polymer composites. However, when producing a polymer nanocomposite with nanoscale conductive filler there are a few ‘keys’ to consider. First, the intrinsic conductivity of the filler material is obviously important. The next two ‘keys’ are filler concentration and geometry, and they work in conjunction to establish a percolation network in the matrix [11]. A percolation network refers to a continuous pathway by which electrons can flow throughout a matrix, which is found through interaction of the filler material. The concentration at which a complete network and complete conductivity has been established is commonly referred to as the ‘percolation threshold’, and it is beneficial to reduce this value as much as possible (Figure 10). Overloading of the filler material can lead to property deterioration. Also, minimizing the need for filler material reduces additional weight to the composite as well as cost.

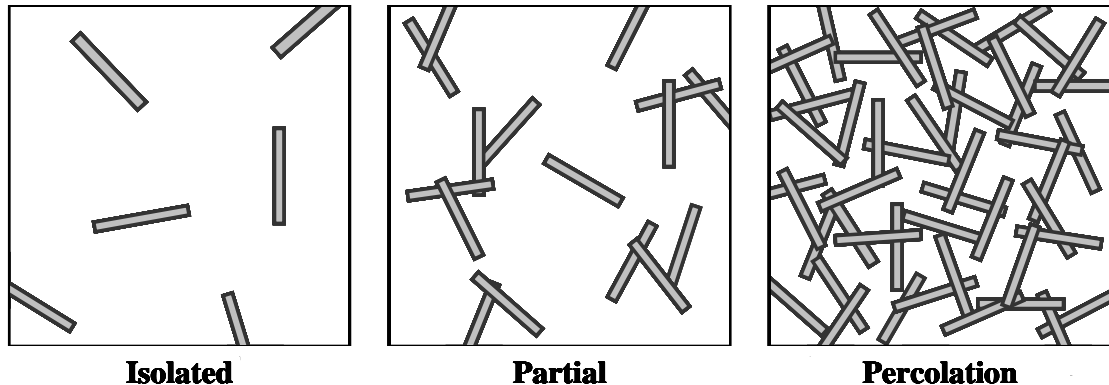


Figure 10. Diagram of a composite filler material percolation network.

CNTs are tremendously attractive as nanoscale filler for these type of materials, because they are able to significantly satisfy all three conditions. With aspect ratios greater than 28,000,000 in the most extreme case [36], but typically between 1,000 – 10,000, the contact ability between nanotubes is extremely high at very low loadings. This keeps down weight, cost, and the reduction of the inherent matrix properties that may result from overloading.

Important to note is that SWNTs potentially offer a better advantage over MWNTs for these materials for several reasons. SWNTs naturally form aligned ‘ropes’ made up of tens to hundreds of nanotubes resting side-by-side and held together by van der Waals forces. These ropes form long three-dimensional conductive pathways that tend to separate and recombine to cover a significant volume in a composite. Also, in electronics it is important to be aware of charge build-up and discharge, because a large discharge can result in damage to equipment. The charge build-up in a composite will depend on the volume of non-conductive space between conductive particles, and the size and geometry of SWNTs reduce these ‘voids’ much better than MWNTs. Last, MWNTs are much more brittle than SWNTs, making them more susceptible to breakage. A build-up of carbon dust, especially in device fabricating clean rooms, from these shards must be avoided as much as possible to prevent damage [11].

Another interesting aspect to briefly mention is the existence of intrinsically conductive polymer materials. Common conducting polymers include polyanilines, polythiophenes, polypyrroles, and polyacetylene. Due to similar temperature dependence, it is believed that conducting polymers behave electrically like a semiconductor. The electrical behavior of conductive polymers is directly related to the order and periodicity

of the atoms, because only ordered molecules produce distinct electron bands. This order depends on the molecular length and regularity of the structure. Conjugated polymers, like polyacetylene, have high crystallinity and high conductivity. A conjugated polymer has alternating single and double bonds between the carbon atoms in the polymer chain. The electrons in the double bond ( $\pi$  electrons) have a weak interaction and can be easily disassociated, which allows for electron flow. For a conjugated polymer structure, if the bonds all have equal lengths, then it results in a metallic band structure. However, the bond lengths are never equal because of the alternation between single and double bonds. This creates a band gap and semiconductor or insulator behavior. The size of the band gap depends on the degree of alternating bond lengths. Often times there is broken symmetry in the bond alternation and two single bonds may meet at a carbon atom. This defect is called a soliton, and it produces a localized non-bonded electron and equal bond lengths at this point. Both of these characteristics create natural conduction and flow. Therefore, in order to improve conductivity, one must attempt to create consistent bond lengths. Another method for improving conductivity is to dope the polymer, similar to the doping of semiconductors. Dopants diffuse between chains and provide charge transfer [37].

Though conducting polymers offer some interesting characteristics, there are several general disadvantages, including poor processability, poor mechanical properties, and poor environmental stability [38]. The processing is very adapted, expensive, and chemically rigorous. The fact that they can not easily withstand excessive handling or manipulation in common environments severely limits their applicability.

## *Applications*

The exceptional and unique properties of CNTs offer a great advantage for the production of improved composites. These nanocomposites can offer extraordinary benefits for an array of applications. Though electrical applications may be the primary focus for the work presented in this report, there are a whole host of thermal, barrier, and mechanical applications that are equally as prevalent and interesting. CNTs have been shown to be a practical polymer reinforcement material by significantly enhancing the toughness, tensile strength, and modulus of a polymer nanocomposite [31-33, 39-43]. These properties make polymer nanocomposites a very viable option for low weight structural materials in various industries, including aerospace, sporting equipment, automotive, and biomedical. At the same time, the extreme thermal stability and thermal conductivity that CNTs have exhibited make nanocomposites equally as viable for many thermal management applications, including as packaging and coatings [32, 43-47].

The electrical applications for these materials are abundant. The most commonly mentioned functions involve electrostatic dissipation, antistatic, EMI shielding, and electrostatic painting. Currently, Hyperion Catalysis International, Inc. offer an assortment of commercial conductive polymer-CNT compounds for automotive and electronic applications [48]. They have produced external body parts (e.g. fenders, door handles) for electrostatic painting and fuel system components (e.g. fuel lines, filter housing) that are electrostatically dissipative and reduce charge build-up. They also offer silicon wafer handling devices (e.g. storage pods, wafer cassettes, tweezers), sockets for testing integrated circuits, and computer disk drive components.

Zyvex Corporation currently offers NanoSolve® Material in the form of additives and concentrates [49]. It is commercially available CNTs or a CNT solution with a range of available solvents that have been treated with a trademarked technology, Kentera™, which non-covalently bonds the CNTs to the polymer matrix to improve dispersion and interaction. They advertise custom CNTs or CNFs as an addition to numerous polymers (e.g. epoxy resins, polyurethane) for applications ranging from golf clubs and adhesives to body armor and electronic packaging.

Additional multi-scale and multi-system applications for CNT-polymer nanocomposites include them being used as field-effect transistors, data storage devices, supercapacitors, photovoltaic cells, electrochromic devices, field emission displays, and electromechanical actuators [50].

## CHAPTER 3

### LITERATURE REVIEW

Polymer nanocomposites with CNT filler have been around almost as long as CNTs themselves, with Ajayan et al. publishing the first report on this topic in 1994 [51]. The interest in this area stems from the fact that polymers offer many desirable qualities, such as toughness, space saving and low weight, good surface finish, flexibility, and low cost. While these properties make polymers useful for electronic device applications, increasing their electrical conductivity from that of an insulator to a semiconductor widens their range even further. By utilizing the superior electrical properties of CNTs [1-9], researchers have shown the great potential for polymer nanocomposites as electroconductive polymers [52-66].

## Electrical Behavior

An issue that arises when attempting to compare the results of numerous researchers is the experimental disparities that exist with respect to processing methods, material choices, and characterization techniques. These variables play very important roles in determining the final properties, and it is almost a requirement that no two reports be exactly alike. Therefore, it is critical to realize that the important, overarching issue is the general role, behavior, and cooperation between polymers and CNTs in the development of improved material properties. It would simply be too ambiguous and incomplete to only report on a consistent, variable-isolated sub-topic, like MWNT composites or melt-processed epoxy resin composites.

The following reports convey the great effectiveness of CNTs to impart enhanced electrical conductivity to a wide range of polymers. Ounaies et al. found a 10 orders of magnitude increase in conductivity with an addition of 0.5 vol.% SWNT, and a percolation threshold of 0.05 vol.% SWNT in a polyimide matrix [52]. Chang et al. observed similar results for a polystyrene (PS)-SWNT nanocomposite, where they showed annealing and sonication can improve dispersion and create a threshold of 0.3 wt.% SWNT [64]. Du et al. reported a percolation threshold of 0.39 wt.% SWNT in a poly(methyl methacrylate) (PMMA) matrix [67].

There are other common filler materials that have been employed as a conductive additive to a polymer matrix, such as carbon black and graphite [68, 69]. When compared to these nanocomposite systems, the difference in polymer-CNT electrical behavior is quite evident. Tang et al. reported a percolation threshold of almost 14 wt.% for a polyethylene (PE)-carbon black composite [68].

Numerous other studies on the electrical behavior of polymer-CNT composites using a variety of polymer matrices have been reported, including PE [62, 63], epoxy resins [59, 60, 70], PS [64, 65, 71], and polypropylene (PP) [58]. Table 2 displays a much more comprehensive view of results from previous electrical studies of CNT nanocomposites.

Table 2. Summary of experimental choices and electrical conductivity results for polymer-CNT nanocomposites.

Polymer	Filler	CNT / Composite Processing	Percolation Threshold	Reference
Polyimide	SWNT	laser ablation / in-situ	0.05 vol.%	[52]
Polyimide	MWNT	CVD / mechanical blending	2.2 vol.%	[53]
PET	MWNT	n/a / precipitation	0.9 wt.%	[54]
PET	SWNT	n/a / melt blending	~2.0 wt.%	[55]
PMMA	SWNT	HiPco / coagulation	0.39 wt.%	[56]
PP	MWNT	CVD / shear mixing	0.05 vol.%	[57]
PP	MWNT	CVD / melt blending	~1.5 wt.%	[58]
Epoxy Resin	MWNT	CVD / in-situ	$\geq 0.017$ vol.%	[59]
Epoxy Resin	SWNT	arc-discharge / in-situ	0.074 wt.%	[60]
Epoxy Resin	MWNT	CVD / shear mixing	0.5 wt.%	[61]
PE	MWNT	CVD / melt blending	7.5 wt.%	[62]
PE	SWNT	n/a / solution adsorption	4.0 wt.%	[63]
PS	SWNT	n/a / solution casting	0.3 wt.%	[64]
PS	SWNT	arc-discharge / freeze drying	1.5 wt.%	[65]
PVA	MWNT	CVD / solution casting	~7.5 wt.%	[66]

## Magnetic Manipulation

CNTs are naturally highly anisotropic because of their high aspect ratios and strong carbon-carbon bonds parallel to the fiber axis. Therefore, common sense would lead one to attempt to take advantage of this behavior by aligning the CNTs to maximize their properties and effect in one direction in a polymer nanocomposite. Numerous alignment techniques have been attempted, including fiber spinning with drawing [72] and/or with a rotating collector [73], shearing [74, 75], plasma-enhanced deposition [76-78], and electric field-induced alignment [79, 80]. Another technique that has gained recent attention is magnetic alignment.

Relatively little research has been completed in the area of magnetically processed polymer-CNT composites, especially thermoplastic composites [70, 81-83]. Kimura et al. showed an increase in electrical conductivity and dynamic modulus parallel to aligned MWNTs when compared to the perpendicular direction in a polyester matrix processed with a 10 Tesla magnetic field [81]. Two other studies which utilized a thermoset epoxy resin are relevant to our study. Choi et al. presented similar results, establishing a 35% decrease in electrical resistivity when an epoxy-SWNT composite was processed with a 25 Tesla field [70]. Last, Camponeschi et al. interestingly reported that CNT alignment was highly matrix dependent and observed enhancements in an array of property areas for an epoxy-based aligned CNT nanocomposite [83]. All of these results present a promising area of research that needs further scrutiny and documentation. Based on information from the literature, it seems that matrix-filler interaction and magnetic field strength are two of the most important variables when attempting to align the CNTs.

To enhance the magnetic susceptibility of CNTs within a polymer matrix, work has been done to attach magnetic nanoparticles to the CNT surface [84, 85]. Correa-Duarte et al. successfully attached iron oxide nanoparticles to CNTs using a polymer wrapping technique and achieved excellent alignment at magnetic field strengths as low as 0.2 Tesla [84]. Shi et al. attached nickel oxide and cobalt oxide nanoparticles to CNFs and produced alignment in a PS matrix with a 3 Tesla applied magnetic field [85].

## PET Nanocomposites

Limited work has been seen in the area of PET-CNT nanocomposites [54, 55, 86-89], with the majority of all PET related research focused on melt processed properties and morphology. Hu et al. actually obtained electrical property results for a precipitated PET-MWNT nanocomposite, showing an increase in conductivity of 8 orders of magnitude and a percolation threshold of 0.9 wt.% MWNT [54]. Shin et al. observed almost a five-fold improvement in the surface resistivity of in-situ polymerized PET-MWNT samples when carboxyl functional groups were used to modify the MWNTs [89]. Anand et al. studied a wide range of properties and behaviors of melt processed and molded PET-SWNT nanocomposites, including crystallization [87] and electrical conductivity [55].

Thus far, no work has been seen in the area of solution cast PET-SWNT nanocomposites, while other solution cast polymer-CNT systems have been studied [90-92]. This lack of attention makes solution casting of particular interest. Also, solution casting offers various advantages as a method for producing thin films, including less need for a thermal stabilizer and larger production equipment (extruder), which reduces processing costs. Solution casting is a factor in the roll-to-roll processing technique often utilized for large-scale manufacturing of printable, flexible electronic devices, such as circuits and solar cells [93, 94].

## CHAPTER 4

### EXPERIMENTAL

#### Materials

PET flakes were purchased from Scientific Polymer Products, Inc. (Ontario, NY), while HiPco processed SWNTs were acquired from Rice University. 1,1,1,3,3,3-Hexafluoro-2-propanol ( $\geq 99\%$ ) (HFP) was purchased from Sigma-Aldrich Co. (St. Louis, MO) to be used as a solvent for the PET polymer.

#### Nanocomposite Film Preparation

##### *Randomly-oriented Films*

Polymer and nanocomposite thin films (thickness,  $t \sim 160 \mu\text{m}$ ) were created using a simple solution blending and casting technique. For the nanocomposite samples (0.5 and 1.0 wt.% SWNT), SWNTs were dispersed in HFP with a Cole-Parmer 8892 ultrasonic bath (frequency,  $\nu = 42 \text{ kHz}$ ) for 4 hours to assure the dispersion of large SWNT aggregations throughout the solvent. PET flakes (1:10 PET/HFP) were placed in the HFP-SWNT solution over heat ( $\sim 75 \text{ }^\circ\text{C}$ ) and continuously mixed with a magnetic stir bar until it appeared that the PET was dissolved in the solution. This was indicated by a visual lack of flakes and an increase in solution viscosity. Solution casting was completed by pouring the solution on top of a glass substrate under a fume hood. A square-shaped polydimethylsiloxane (PDMS) barrier (height,  $h = 859 \mu\text{m}$ ) was used to

contain and shape the solution and subsequent film. A doctor's blade was used to level the solution to the barrier height. One large film (area,  $A = 400 \text{ cm}^2$ ) of each sample type was produced. Once the solvent had evaporated and crystallization was completed, the film was placed in a Curtin Matheson Scientific, Inc. Equatherm vacuum oven at approximately  $90 \text{ }^\circ\text{C}$  to assist in the removal of any residual solvent in the film. Figure 11 shows the processing flow chart, and Figure 12 shows a digital image of various PET films which were solution cast with SWNT loadings of 0.0, 0.5, and 1.0 wt. %.

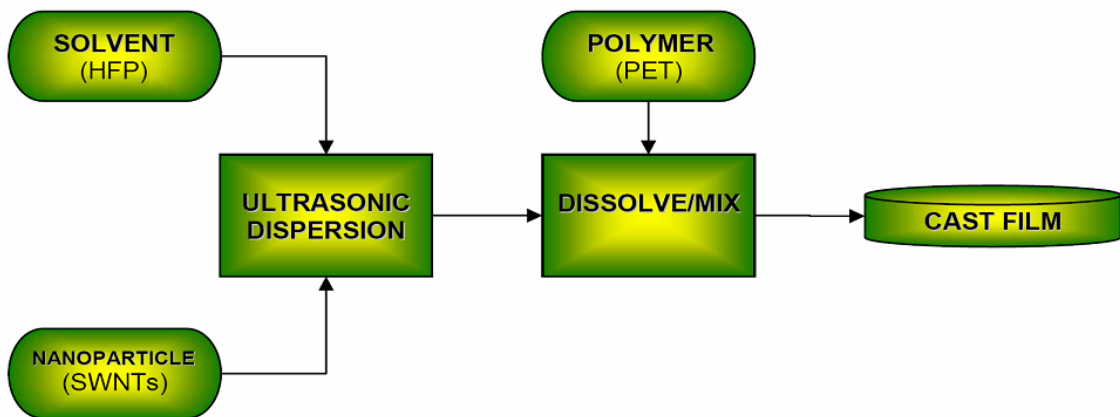


Figure 11. Film processing flow chart.

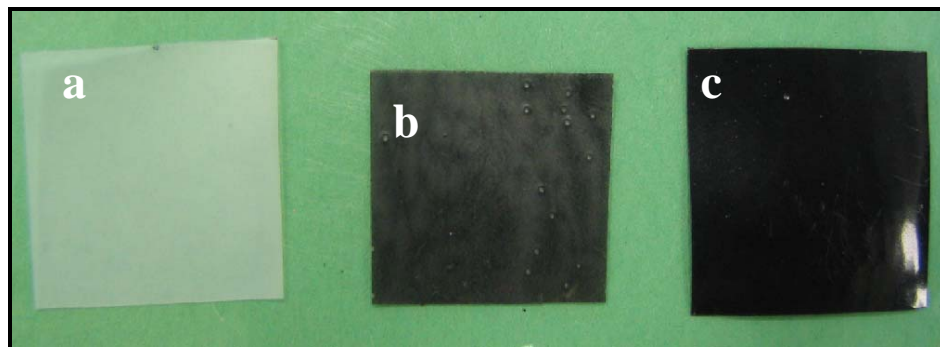


Figure 12. Digital image of solution cast PET films of varying SWNT loadings (a) 0.0 wt.% SWNT, (b) 0.5 wt.% SWNT, and (c) 1.0 wt.% SWNT.

## *Magnetically Aligned Films*

The aligned films were produced in the same manner as the unaligned films, except after the PET-SWNT solutions were poured onto a glass substrate they were subsequently placed in a large magnetic resonance imaging (MRI) scanner. Two separate MRI scanners were used, each producing different magnetic field strengths (3 Tesla and 9.4 Tesla). A Siemens Magnetom Allegra was used to produce a 3 T magnetic field, while a Bruker BioSpec® was also used and produced a 9.4 T magnetic field. The magnetic field direction is parallel to the long axis of the core of the scanner (Figure 13).

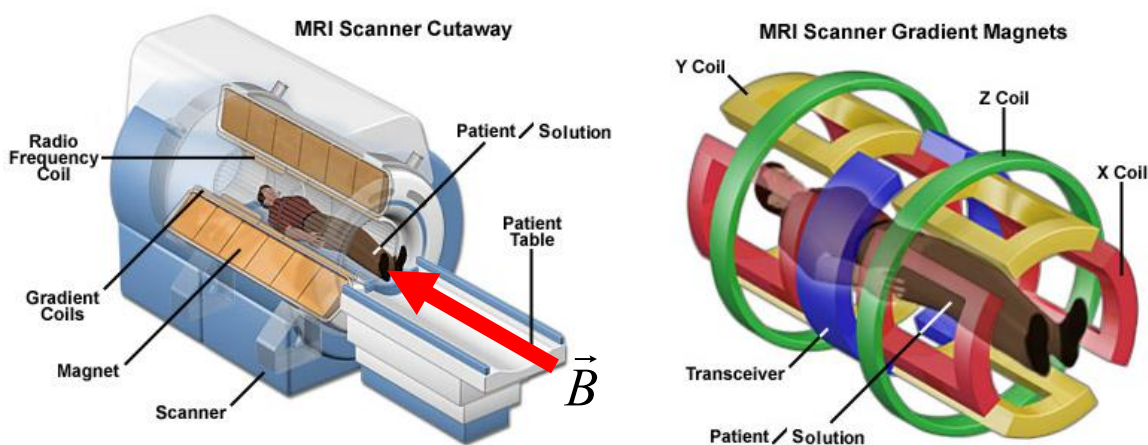


Figure 13. Diagrams of a representative MRI scanner showing the arrangement of the superconducting magnets and specimen placement. From “MRI: A Guided Tour” by K.E. Coyne, 2006, [www.magnet.fsu.edu](http://www.magnet.fsu.edu). Copyright 2006 by the National High Magnetic Field Laboratory. Reprinted with permission.

## SWNT Characterization

### *Transmission Electron Microscopy (TEM)*

TEM micrographs were acquired with a FEI Tecnai™ G<sup>2</sup> Spirit microscope. Pristine SWNTs and PET-SWNT nanocomposite films were imaged using TEM.

Prefabricated, Formvar® coated grids were used to help image the pristine SWNTs. Each film type was microtomed prior to imaging, parallel and perpendicular to the largest surface area plane. TEM was used to qualitatively characterize nanotube aspect ratio and tube-to-tube interaction in the form of nanotube bundles.

### *Raman Spectroscopy*

Raman spectroscopy was performed with a Renishaw inVia microRaman microscope. It was used to characterize SWNT diameter and the effect of sonication on nanotube integrity. Samples of SWNTs were sonicated in HFP for varying amounts of time (0, 1, 2, 4, and 6 hours), then each respective Raman spectrum was quantitatively analyzed with respect to the commonly accepted D-peak ('disorder peak') found around  $1300\text{ cm}^{-1}$  and the radial breathing mode between  $100$  to  $400\text{ cm}^{-1}$ . Spectra were acquired with 488 and 785 nm excitation wavelengths for the diameter study, but only 785 nm was used for the sonication study. The power used was 1.25 mW for the diameter study and 0.5 mW for the sonication study. A 50x objective lens, 20 second accumulation time, and 3 accumulations were used for all studies.

## Crystallization Behavior Characterization

### *Instrumentation and Setup*

Differential scanning calorimetry (DSC) was used to study the isothermal and non-isothermal crystallization characteristics of the PET-SWNT nanocomposites. The instrument employed was a TA Instruments DSC Q-100, with indium used for temperature calibration ( $T_m = 156.6^\circ\text{C}$ ,  $\Delta H_m = 28.4\text{ J/g}$ ). An empty pan was used as a

reference. Five samples (5-10 mg) from each film type were placed in aluminum pan bottoms and measurements were taken in a nitrogen environment. The tops of the DSC pans were not used, because it was determined that small amounts of residual solvent present in the samples would condense on the inside portion of the tops then drip back into the molten sample over the course of the DSC experiment. By running the samples in an open pan, the residual solvent was able to evaporate away from the sample without affecting the crystallization process.

#### *Non-isothermal Crystallization*

Non-isothermal protocol consisted of heating a sample above the melting temperature to 300°C, and then allowing it to stand at that temperature for 30 minutes to erase any thermal history and remove residual solvent. Non-isothermal crystallization measurements were then taken as a sample was cooled at a rate of 10°C/min to room temperature. Analysis of variation (ANOVA) was performed to test the significance of the results.

#### *Isothermal Crystallization*

Isothermal protocol began by heating a sample in the same manner as the non-isothermal protocol and leaving it at 300°C for 30 minutes. The maximum cooling rate allowed by the instrument (60°C/min) was then implemented to reach each crystallization temperature quickly and to avoid as much premature crystallization as possible. Several different crystallization temperatures were used (200, 205, 210, 215, 220, 225, and 230°C), and each was maintained for 10 minutes. Once again, ANOVA was completed.

## Magnetic Alignment Characterization

The primary mechanism for characterizing the alignment of the SWNTs within the PET matrix was Raman spectroscopy. Raman spectra were obtained for the magnetically aligned nanocomposite samples (0.5, 1.0, and 3.0 wt.% SWNT). The tangential mode, or G-peaks ( $\sim 1600\text{ cm}^{-1}$ ), of these spectra were highlighted and analyzed with respect to degree of SWNT orientation in the films. Each sample was measured at several different angles with respect to the direction of the magnetic field, with 0 degrees corresponding to a direction parallel to the magnetic field and 90 degrees being perpendicular to the field. The experimental parameters include using a 785 nm excitation wavelength, a power of 0.1 mW, a 50x objective lens, a 20 second accumulation time, and 3 accumulations per direction per sample.

Also, TEM was used to gather a qualitative understanding of the SWNT alignment. Each sample type was microtomed, and micrographs were acquired at various magnifications.

## Impedance Spectroscopy

The AC electrical impedance of the PET-SWNT nanocomposites was measured with a Hewlett Packard 4284A Precision LCR Meter at room temperature. Measurements were acquired across a frequency range of 20 Hz to  $10^6$  Hz. Each aligned sample was measured parallel to the direction of the magnetic field that was placed upon it during processing.

CHAPTER 5  
RESULTS AND DISCUSSION

SWNT Morphology

Determining the morphology of CNTs is vital for analyzing and correlating with the results of property characterization. The SWNTs used in this study were acquired from Rice University and produced with the HiPco process. TEM images of pristine SWNTs clearly show a very high aspect ratio and strong tube-to-tube interaction, resulting in much bundling of the nanotubes (Figure 14). The extremely small dimensions and bundling of the SWNTs makes it very difficult to measure their size with a high degree of certainty, due to the lack of good image resolution along the edges/walls of the nanotubes.

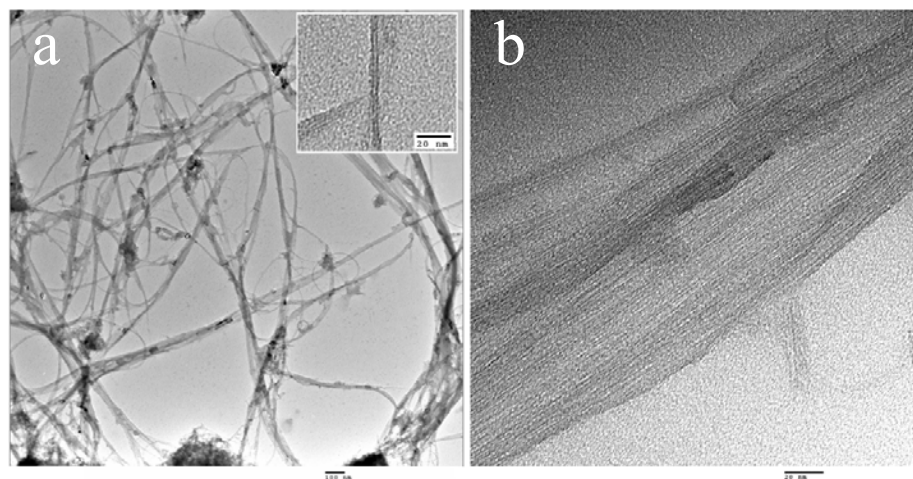


Figure 14. TEM micrographs of pristine SWNTs showing (a) high aspect ratios, *Inset*. Isolated SWNTs with small dimensions ( $d \sim 1-4$  nm), and (b) bundling.

Another method for determining SWNT size that is often utilized is Raman spectroscopy. The Raman spectrum of a SWNT is very unique, and it includes a radial breathing mode (RBM) region between 100 and 400  $\text{cm}^{-1}$ . The RBM frequency is specific to SWNTs, and it corresponds to in-phase radial vibrations of the atoms with respect to the nanotube axis, which results in a monotonic, inverse relationship to nanotube diameter. The RBM frequency ( $\nu_{\text{RBM}}$ ) correlates with individual tube diameter ( $d_{\text{SWNT}}$ ) through the following relation [95, 96]:

$$\nu_{\text{RBM}} = \frac{223.5}{d_{\text{SWNT}}} + 12.5 \quad (1)$$

Figure 15 shows the Raman spectra of the SWNTs at two different excitation wavelengths (488 nm and 785 nm), with some of the frequency peaks ( $\nu_{\text{RBM}}$ ) used for analysis properly labeled (*insets*). Multiple laser excitations were used, because each can selectively excite different nanotubes with specific diameters. This provides a larger sample distribution. Based on (1), the range of SWNT diameters was determined to be 0.58 – 1.53 nm with the average SWNT diameter being  $1.05 \pm 0.33$  nm. This size distribution agrees satisfactorily with previous reports of SWNT size produced with the HiPco process [97, 98].

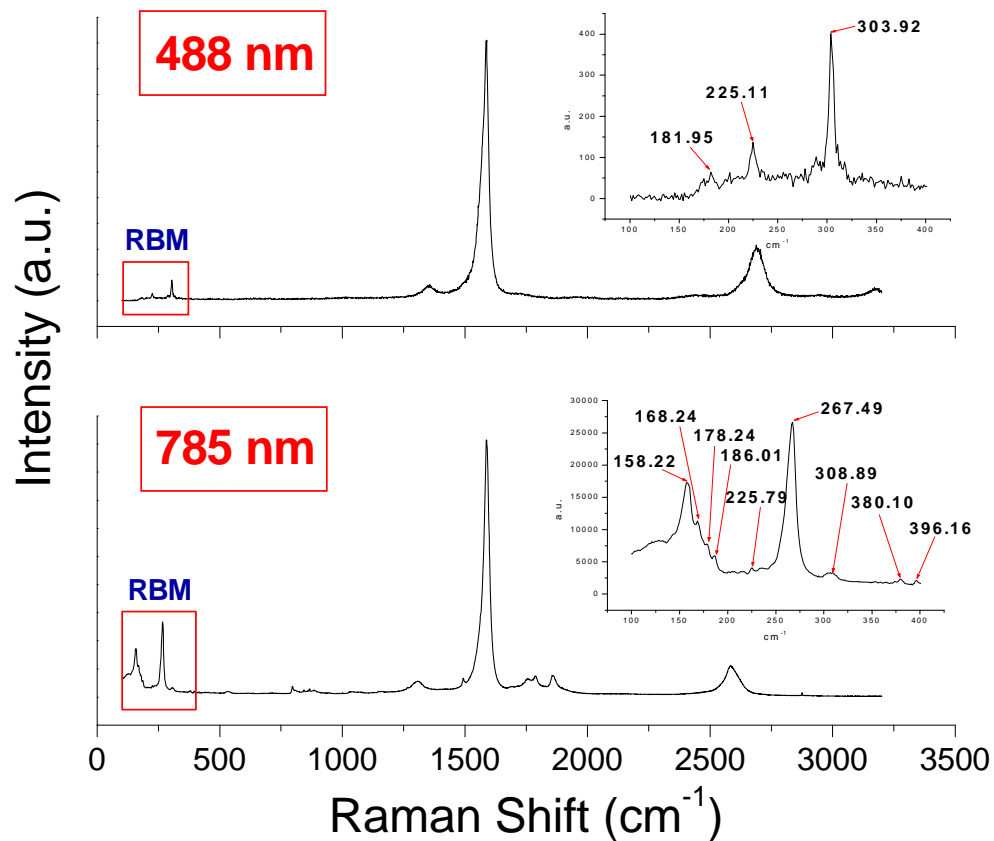


Figure 15. Raman spectra of SWNTs with varying laser excitation wavelengths (488 and 785 nm). *Insets.* RBM regions with labeled frequency peaks.

Besides determining nanotube size, Raman spectroscopy is also very useful for interpreting the integrity of the nanotubes. This is observed through another important spectrum feature for SWNTs known as the D-peak (‘disorder peak’), centered around  $1300\text{ cm}^{-1}$ . This feature is attributed to an increasing amount of defects or disorder inducing artifacts, which can include amorphous carbon, holes, or impurities. It has been reported that excessive sonication during dispersion, or sonication in a hostile solvent, can result in chopping and an increase in defects in CNTs [99, 100]. This will produce an

increase in the D-peak intensity. Damaging the SWNTs is unwanted because it will lead to poor property enhancement in the nanocomposite film. Figure 16 shows the Raman spectra of SWNTs sonicated for various amounts of time between 0 and 6 hours.

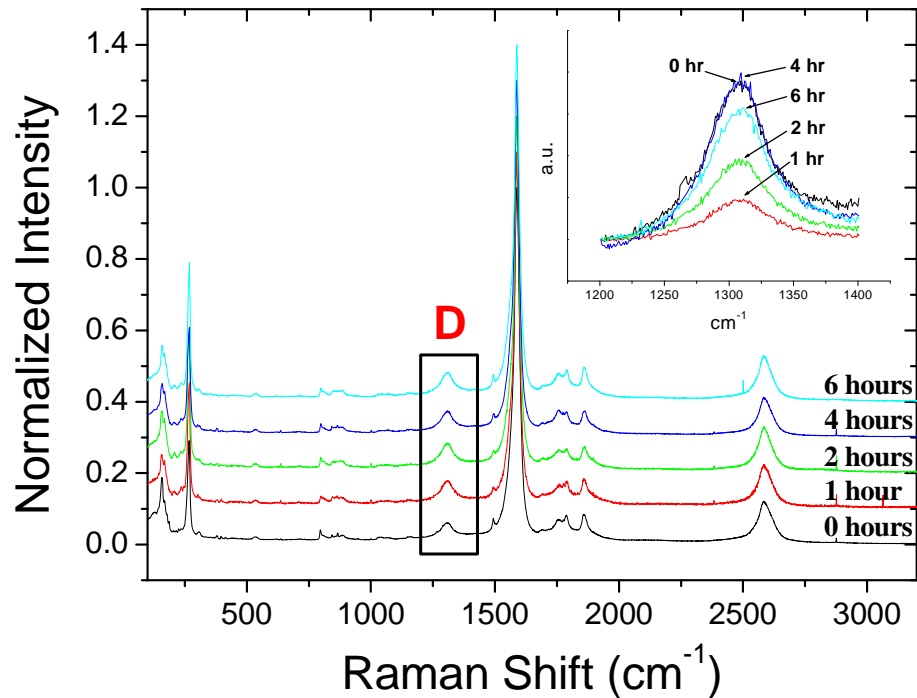


Figure 16. Raman spectra of SWNTs sonicated for varying time periods (0-6 hours). *Inset.* D-peaks of each spectrum between 1200 and 1400 cm<sup>-1</sup>.

The spectra show minute differences in the peak intensities of the D-peaks. Also, there does not seem to be a correlation between sonication time and peak intensity. It can be reasonably assumed then that any difference in intensity is due to sample to sample variation, and it is not dependent upon sonication time. Therefore, integrity was not compromised in any way by dispersing them in an ultrasonic bath for 4 hours during film processing.

## Crystallization Behavior

The DSC experiments were performed on three samples of PET film, each with varying concentrations of SWNTs. These included a neat PET film, void of SWNTs, and two nanocomposite PET films with 0.5 and 1.0 wt.% SWNT. It is important to look at the crystallization behavior of a polymer, because the crystallization helps determine the physical state, and thus the final properties. The crystallization of PET has been studied extensively [101-106]. Several studies have shown CNTs to affect the crystallization behavior of PET, particularly when crystallized from the melt [87, 88].

Figure 17 shows the non-isothermal exotherms of each film type at a single cooling rate ( $10^{\circ}\text{C}/\text{min}$ ). The crystallization induction temperature ( $T_o$ ), crystallization peak temperature ( $T_c$ ), and percent of crystallinity are reported in Table 3.

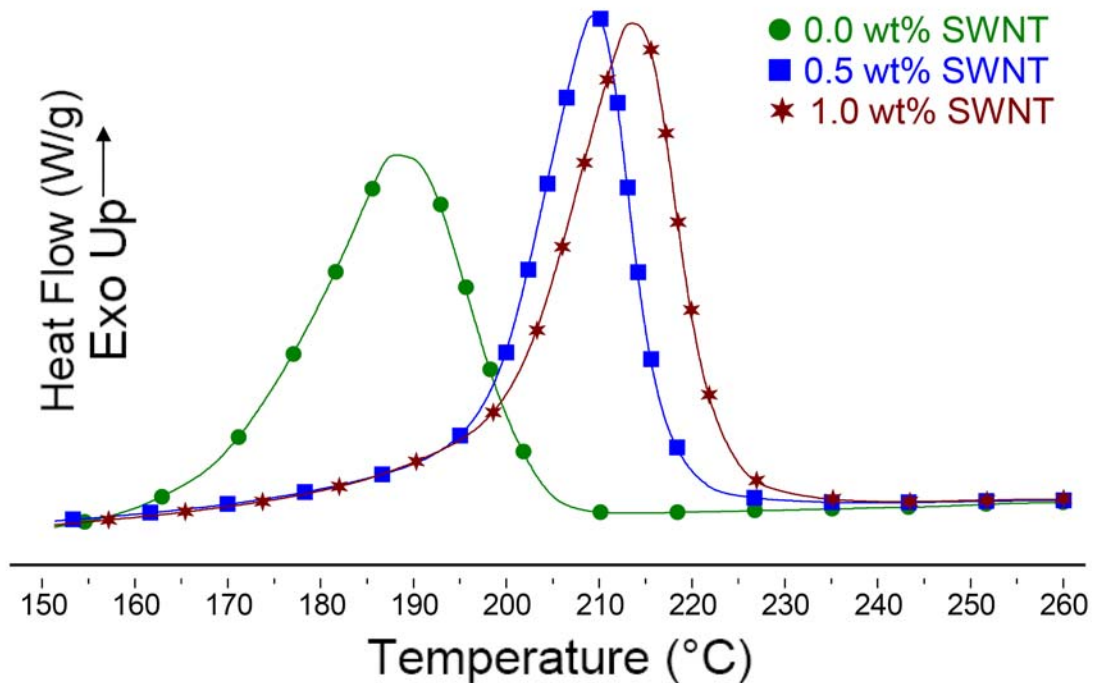


Figure 17. DSC scans of heat flow vs. temperature during non-isothermal crystallization of various PET-SWNT composites at a cooling rate of  $10^{\circ}\text{C}/\text{min}$ .

Table 3. Non-isothermal crystallization parameters for PET and PET-SWNT composites (n=5), and p-values (ANOVA) with respect to SWNT concentration.

Sample (wt%)	T <sub>o</sub> (°C)	T <sub>c</sub> (°C)	Crystallinity (%)
0.0	203.2 ± 1.0	188.7 ± 1.3	26.0 ± 1.0
0.5	217.2 ± 0.6	209.3 ± 0.5	27.6 ± 2.0
1.0	222.7 ± 0.6	213.8 ± 0.8	28.9 ± 1.2
<i>Significance (p-value)</i>	< 0.0001	< 0.0001	< 0.0241

Based on these results, the addition of SWNTs significantly affected the non-isothermal crystallization behavior by increasing the T<sub>c</sub> approximately 20°C with the addition of 0.5 wt.% SWNT and 25°C by adding 1.0 wt.% SWNT. From these results, it can be stated that the addition of very small amounts of SWNTs can lead to a very strong nucleating effect. Also, as the SWNT concentration increases, the rate of crystallization temperature change seems to decrease. This signifies a decrease in the nucleating efficiency due to increasing saturation of nucleation sites. This may be directly related to SWNT concentration alone, or it may also be dependent on dispersion and degree of SWNT bundling. Smaller, well dispersed nucleating units will result in a higher number of nucleating sites and earlier crystallization.

The previously mentioned effect, along with several other potential factors, may be the causes for the relatively low crystallinity seen in the samples. Crystallinity is easily determined from the melting exotherms (not shown) of DSC scans with the following equation:

$$X_C = \frac{\Delta H_f}{\Delta H_f^0} \quad (2)$$

Where  $\Delta H_f$  is the enthalpy of fusion of each sample, and  $\Delta H_f^0$  is the enthalpy of fusion of a 100% crystalline material. The increase in crystallization rate caused by a large number of nucleating sites from many well dispersed SWNTs could have an adverse secondary effect on the mobility of PET chains. The nano-confinement of the polymer chains caused by the CNT interaction and dispersion can greatly inhibit chain mobility and extended crystallite formation.

Also, the processing method is unfavorable for stress-induced molecular orientation and crystallization. Solution casting, as opposed to solution spinning, roll-to-roll processing, or melt processing, is very stress-free. The solution is not being forced out of a spinneret, drawn onto a collector, or given a lot of thermal energy that would allow for easier chain mobility. Another processing factor may be the quick evaporation of the solvent. HFP has a relatively low boiling point ( $\sim 58^\circ\text{C}$ ) and is almost completely removed from the material in under one hour at room temperature. This quick gelation of the solution would make it very difficult for the polymer chains to naturally orient themselves into large crystallites.

Figure 18 shows isothermal crystallization exotherms of each sample for, at most, seven crystallization temperatures. Only four crystallization temperatures are seen for the 0.0 wt% SWNT sample, because the crystallization times of the highest crystallization temperatures (220 – 230°C) exceeded the maximum allotted time (10 min.) allowed for the experiment. Exact values can be found in Table 4.

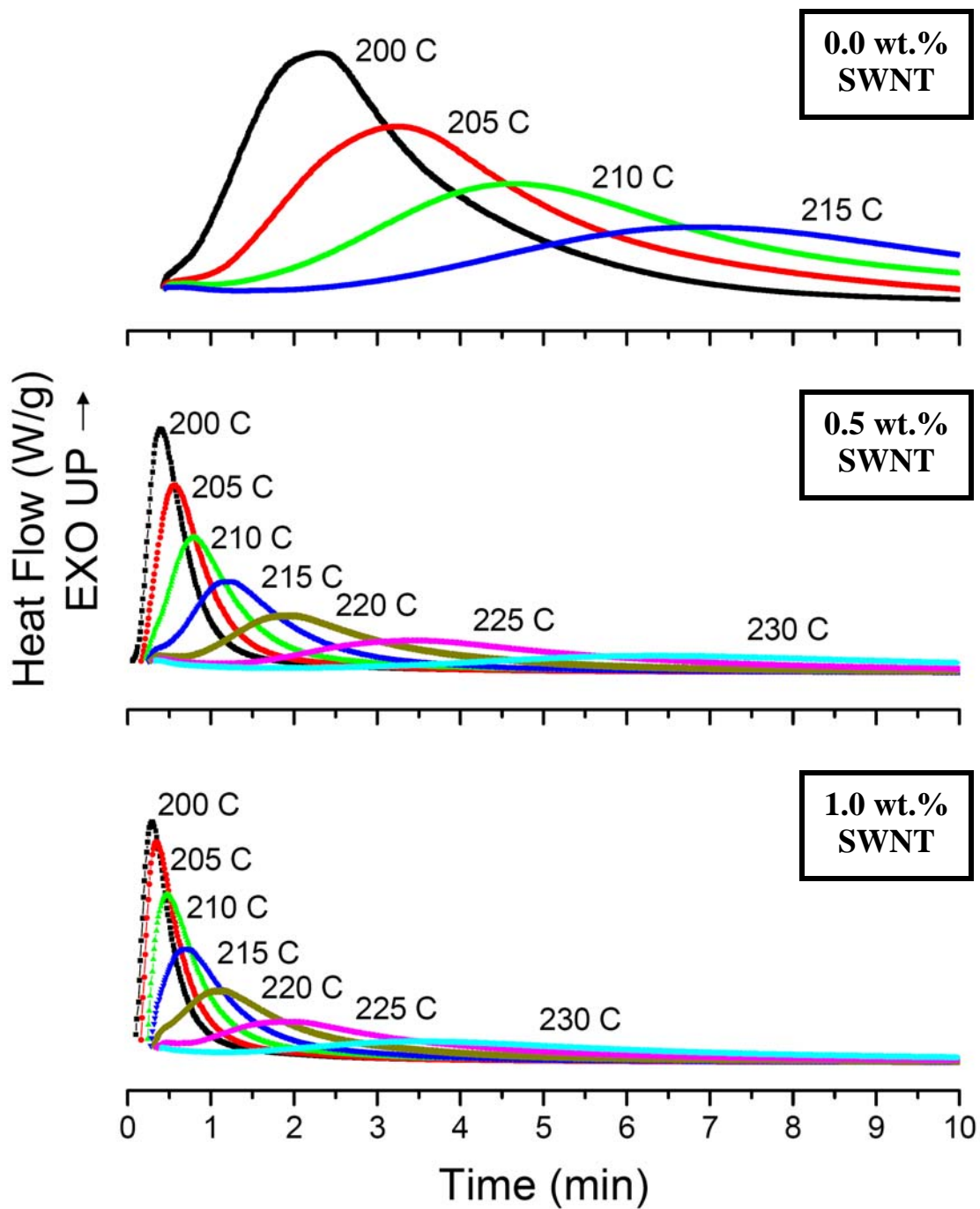


Figure 18. DSC scans of heat flow vs. time during isothermal crystallization of various PET-SWNT composites at different crystallization temperatures.

Table 4. Average values for isothermal crystallization times (min.) of PET-SWNT films (n=5), and p-value (ANOVA) for each crystallization temperature with respect to SWNT concentration.

Sample (wt%)	200 °C	205 °C	210 °C	215 °C	220 °C	225 °C	230 °C
0.0	2.3 ± 0.2	3.2 ± 0.2	4.6 ± 0.3	6.8 ± 0.4	---	---	---
0.5	0.4 ± 0.0	0.6 ± 0.0	0.8 ± 0.0	1.2 ± 0.1	2.0 ± 0.1	3.5 ± 0.2	6.5 ± 0.3
1.0	0.3 ± 0.0	0.4 ± 0.0	0.5 ± 0.0	0.7 ± 0.0	1.2 ± 0.1	2.0 ± 0.1	3.8 ± 0.3
<i>Significance (p-value)</i>	< 0.0001	< 0.0001	< 0.0001	< 0.0001	< 0.0001	< 0.0001	< 0.0001

These isothermal crystallization results show a significant SWNT effect on the crystallization time at concurrent crystallization temperatures. At 200° C, the crystallization time was reduced by 81% by adding 0.5 wt.% SWNTs and 87% with the addition of 1.0 wt.% SWNT. Once again, the increase in crystallization occurs at the same time a decrease in rate of change with increasing SWNT loading occurs. This further supports the notion that SWNTs greatly increase the crystallization rate of the PET films. At the same time, a SWNT saturation limit is approached, and the SWNT will cease supporting nucleation and growth and begin to have a negative consequence.

The significantly large increase in crystallization rate with relatively low SWNT loading is very promising and beneficial for commercial applications where fast production cycle times are required. However, applications requiring specific properties and/or highly crystalline products may need to follow a different processing method, possibly melt or high stress solution processing. Roll-to-roll processing could help in this regard. A solvent-polymer system with slower gelation may also be a solution.

## Magnetic Alignment

Due to their magnetic susceptibility [23-29], it should be possible to place SWNTs in a magnetic field and align them in a common orientation parallel to the field direction. The variables that must be accounted for in this endeavor are the effects of the polymer matrix and tube-to-tube interactions. Raman spectroscopy is once again a vital tool when attempting to characterize the degree of alignment of SWNTs in a polymer matrix. Another Raman feature of SWNTs can be found around  $1600\text{ cm}^{-1}$ . This peak is commonly referred to as the tangential mode (TM), or G-peak, and is due to elongations of the carbon-carbon bonds along the longitudinal axis of the CNT. Therefore, if the CNTs are aligned, there should be an increase in the G-peak intensity when they are parallel to the polarized laser excitation plane (Figure 19).

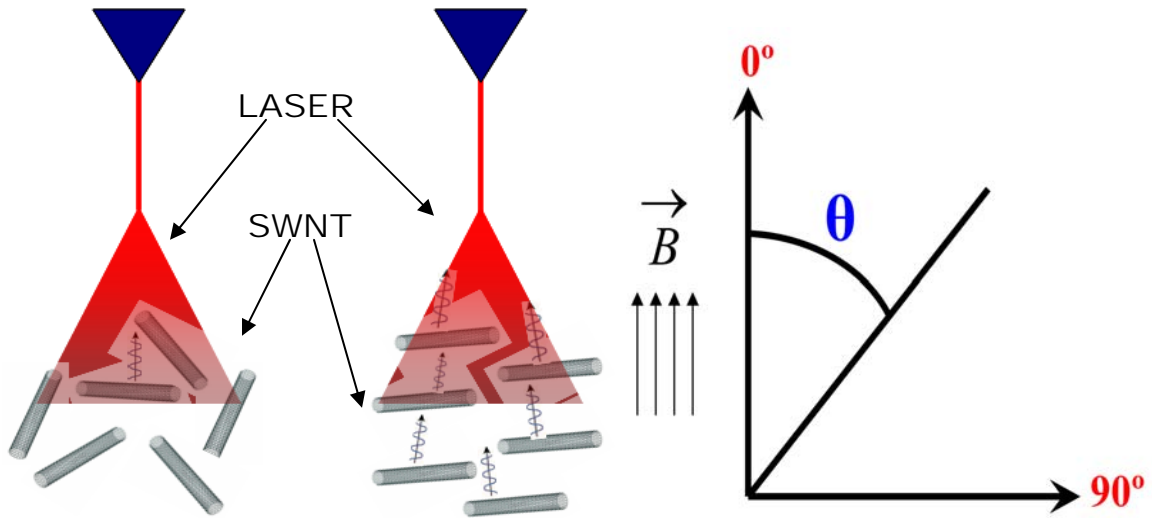


Figure 19. Diagrams showing unaligned/aligned CNT response to an excitation laser and sample orientation notation relative to an applied magnetic field during processing.

Figure 20 presents the G-peaks of a representative example of an unaligned film. Each peak is identical and independent of the measurement angle, which illustrates the isotropic nature of the CNTs within the nanocomposite. Figure 21 shows the G-peak intensities for 0.5, 1.0, and 3.0 wt.% SWNT samples processed under a 3 Tesla (top of Figure 20) and 9.4 Tesla (bottom of Figure 20) magnetic field at varying orientation angles [0 degrees is parallel to the magnetic field and 90 degrees is perpendicular to the magnetic field (Figure 19)]. An additional, higher SWNT concentration sample (3.0 wt.% SWNT) was prepared in order to gain a better understanding of the effect that SWNT concentration has on orientation.

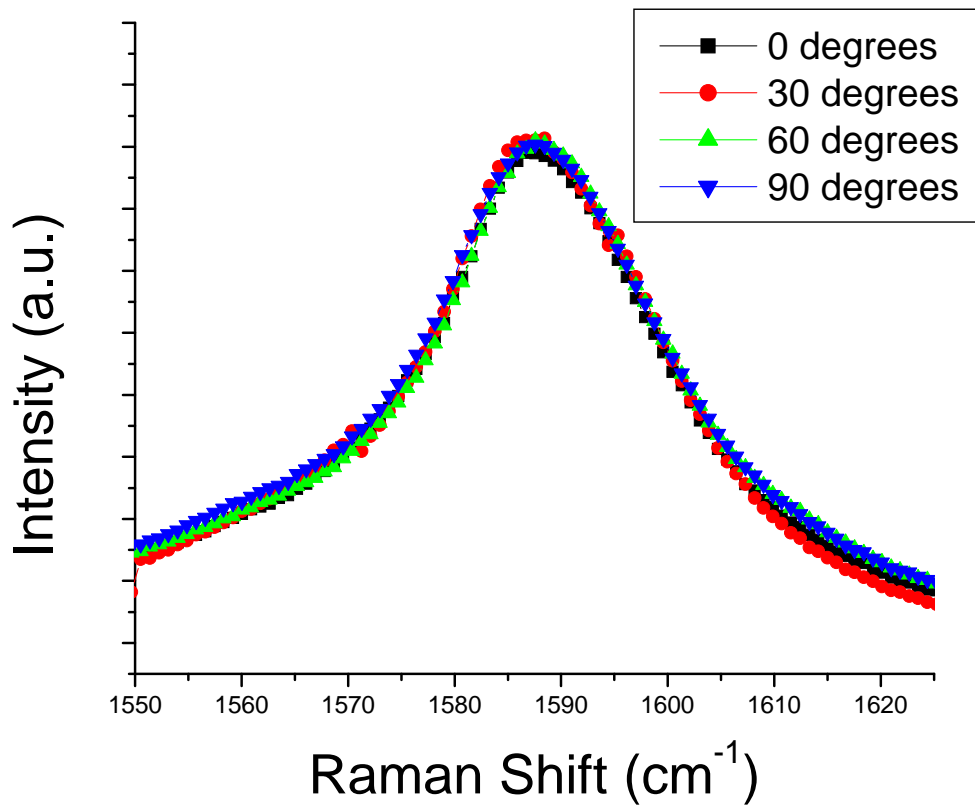


Figure 20. G-peak spectra of an unaligned PET-SWNT nanocomposite film showing the independence of the measurement angle relative to the orientation of the SWNTs.

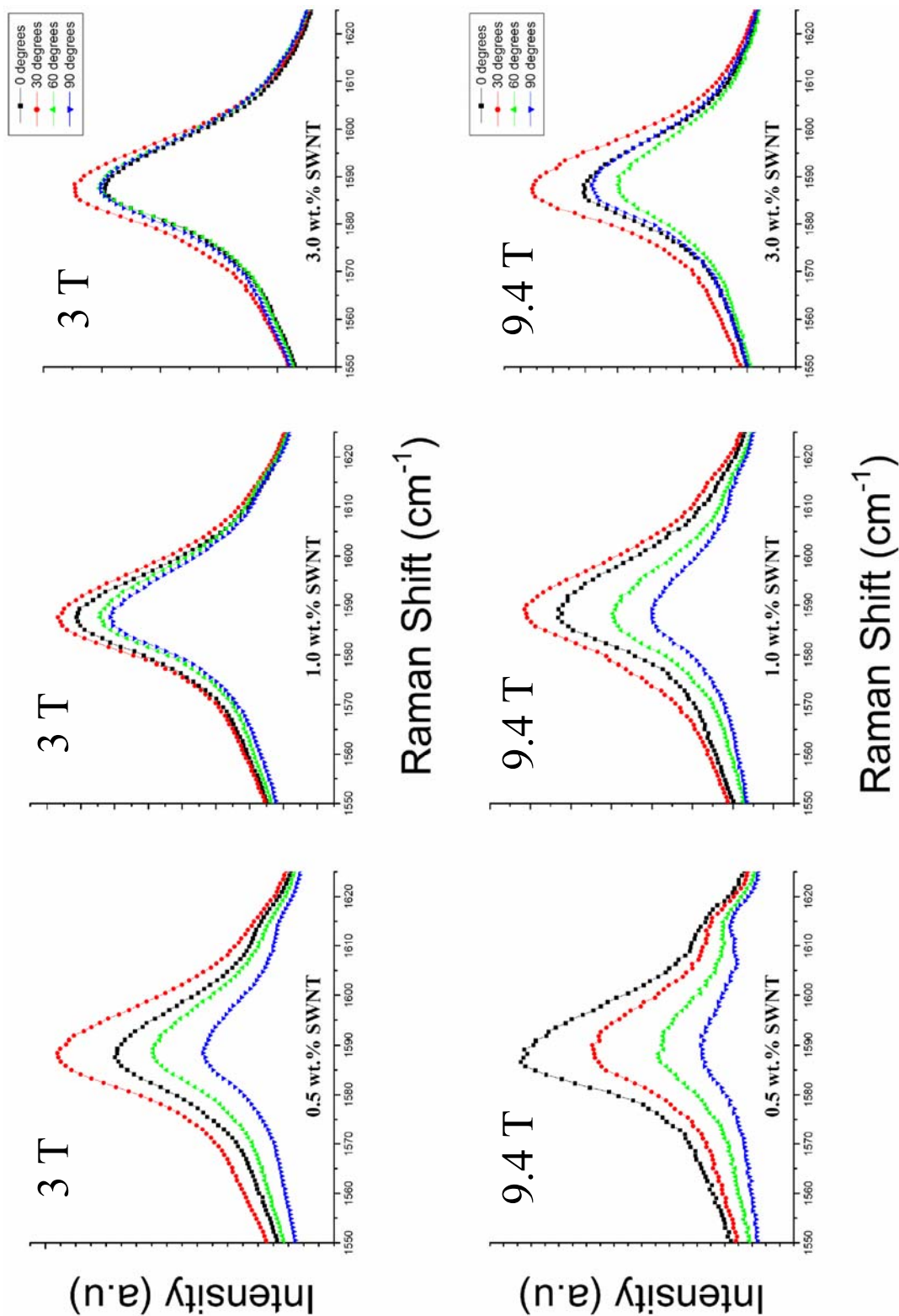


Figure 21. G-band intensities relative to the magnetic field direction (0 degrees = parallel) of Raman spectra for samples with varying SWNT loadings and magnetic field processing parameters.

The spectra present some very interesting results about the effect of magnetic field strength and SWNT concentration on orientation. Both seem to play a very important role in completing SWNT alignment. An ideal case (perfect alignment along the direction of the magnetic field for 100% of the SWNTs) would produce a Raman spectrum with an incredibly great G-peak intensity parallel to the magnetic field (0 degrees), and extremely minute to almost flat (no intensity) peaks for every other orientation.

The G-peak intensity results of this study present incomplete alignment for all three SWNT concentrations processed with a 3 Tesla magnetic field, with the primary orientation being approximately 30° off-parallel. Also, the peak spacing between each orientation (0° - 90°) give a good visual representation of the anisotropy of the SWNTs in the PET matrix. As the SWNT concentration increases, there is a decrease in the peak spacing which corresponds to a more isotropic behavior. This is most likely caused by increasing restrictions on SWNT mobility due to an increase in solution viscosity and nanotube bundling/interactions. Alignment with a much stronger magnetic field (9.4 Tesla) supports this idea. Important to note is that a 9.4 Tesla magnetic field is able to overcome the obstacles that inhibited complete alignment at a low SWNT concentration (0.5 wt.%), while the more isotropic behavior at higher concentrations is less prominent. The peak spacing is further apart for the 9.4 Tesla processed samples as compared to their 3 Tesla counterparts, which means the higher field strength is able to produce more aligned samples at higher SWNT concentrations. This behavior can be visually interpreted through digital TEM micrographs showing the extent of SWNT alignment as a function of magnetic field strength (Figure 22).

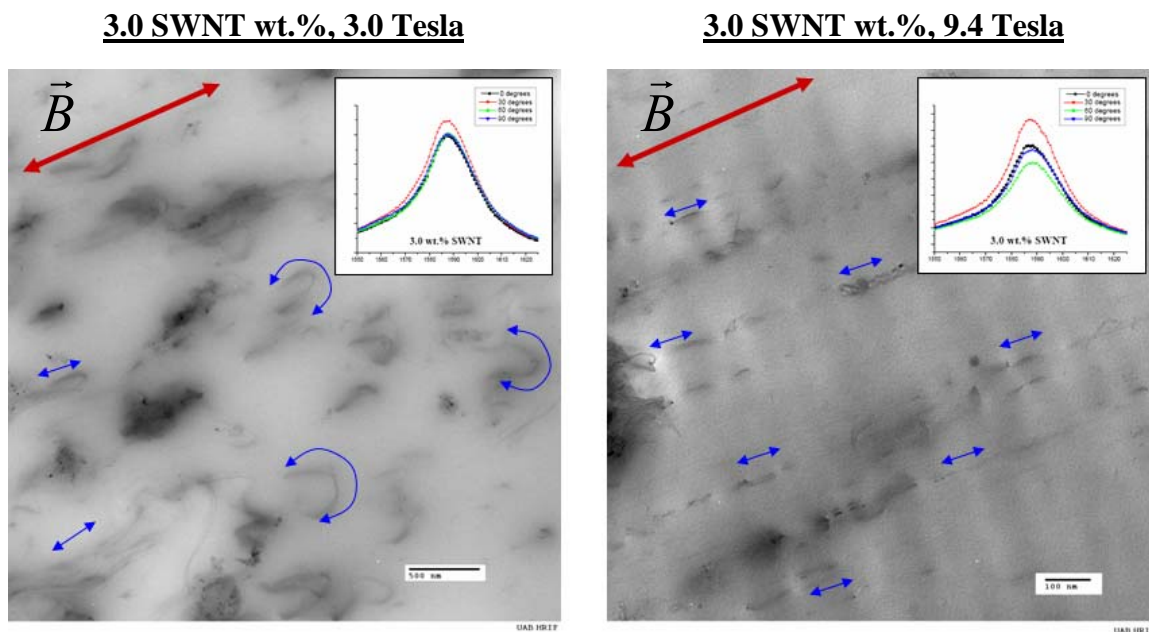


Figure 22. TEM micrographs showing the effect of magnetic field strength at a constant SWNT loading (3.0 wt.%).

The micrographs present a qualitative measurement of the effect of magnetic field strength on SWNT alignment within a PET matrix. The 3.0 wt.% SWNT sample processed at 3 Tesla shows slight, generalized alignment of the SWNTs while a large quantity of the nanotubes are unextended. Due to the manner in which many of the SWNTs in the micrograph appear bent but directed towards the direction of the magnetic field, it would seem to indicate that the SWNTs were in the process of aligning to the field but were not able to completely extend before gelation. The resistive forces were too great for a weaker magnetic field to completely overcome them in the allotted processing time. This also implies that an adjusted solution-based sample preparation process with a slower gelation (slower solvent evaporation) may yield aligned SWNTs with only a 3 Tesla magnetic field. A stronger magnetic field was able to induce the SWNTs to extend and align in a much shorter amount of time.

Therefore, it appears that magnetic alignment is possible and can partially occur under magnetic field strengths as low as 3 Tesla, with the SWNT concentration and magnetic field strength playing important roles in determining the degree of orientation. Though a 3 Tesla magnetic field was not able to achieve complete alignment, even at low SWNT loadings, the samples processed at this parameter may still prove to be a very effective conductive material. It has been reported that complete alignment may not be ideal for enhancing conductivity, due to an increase in void space between nanotubes [56, 107]. Straight lines of SWNTs do not agree with the model of an interconnecting network that produces percolation. Improving SWNT behavior by taking advantage of their anisotropic nature while reducing void space and nanotube-to-nanotube distance with only slight alignment (30° off-parallel) could potentially produce the best electrically conductive behavior [74, 108].

## Impedance Spectroscopy

Impedance spectroscopy is a compelling method for characterizing many of the electrical properties of materials and their interfaces. It may be used to investigate the dynamics of electron charge flow in the bulk or interfacial regions of various kinds of solid composites [i.e. ionic, semi-conducting, and even insulators (dielectrics)]. In this study, an electrical stimulus is applied to a polycrystalline material (PET) and the response is observed with a HP 4284A Precision LCR Meter at room temperature. It is assumed that the properties of the material system are time-invariant. The purpose of impedance spectroscopy is to determine the electrical response, property interrelations, and the dependence of the properties on such controllable variables as applied voltage and filler concentration for composite systems.

A large number of processes take place throughout a nanocomposite when it is electrically stimulated, which will have a strong effect upon the overall electrical response. They include the transport of electrons through the CNT conductors, across CNT-polymer interfaces, and between grain boundaries. Impedance ( $Z$ ) is analogous to resistance, and it is a measurement of a systems total opposition to alternating current (AC) flow caused by these various transport circumstances. It is an extension of resistance by including capacitive and inductive components to the system, and it modifies Ohm's Law in the following manner:

$$I = \frac{V}{Z} \quad (3)$$

Current (I) is now proportional to voltage (V) divided by impedance. Current and voltage are still in units of amperes and volts, respectively, while impedance is measured in ohms.

The LCR meter used for impedance spectroscopy obtains profiles of the AC complex impedance ( $Z^*$ ) as a function of frequency. From these measurements the complex admittance ( $Y^* = 1/Z^*$ ) can be determined and modeled as a parallel resistor (R) and capacitor (C). It can be written as a function of frequency ( $\omega$ ) and takes the following form:

$$Y^*(\omega) = Y' + jY'' - \frac{1}{R} + j\omega C \quad (4)$$

The specific AC conductivity of the PET-SWNT nanocomposites as a function of frequency [ $\sigma(\omega)$ ] is calculated from the complex admittance:

$$\sigma(\omega) = |Y^*(\omega)| \frac{t}{A} \quad (5)$$

The other parameters,  $t$  and  $A$ , are the thickness and cross-sectional area, respectively, of the tested sample.

### *Results*

Figure 23 shows the AC conductivity plots for the various PET-SWNT nanocomposites. The plots include randomly-oriented and aligned sample types at 3 Tesla and 9.4 Tesla magnetic field strengths.

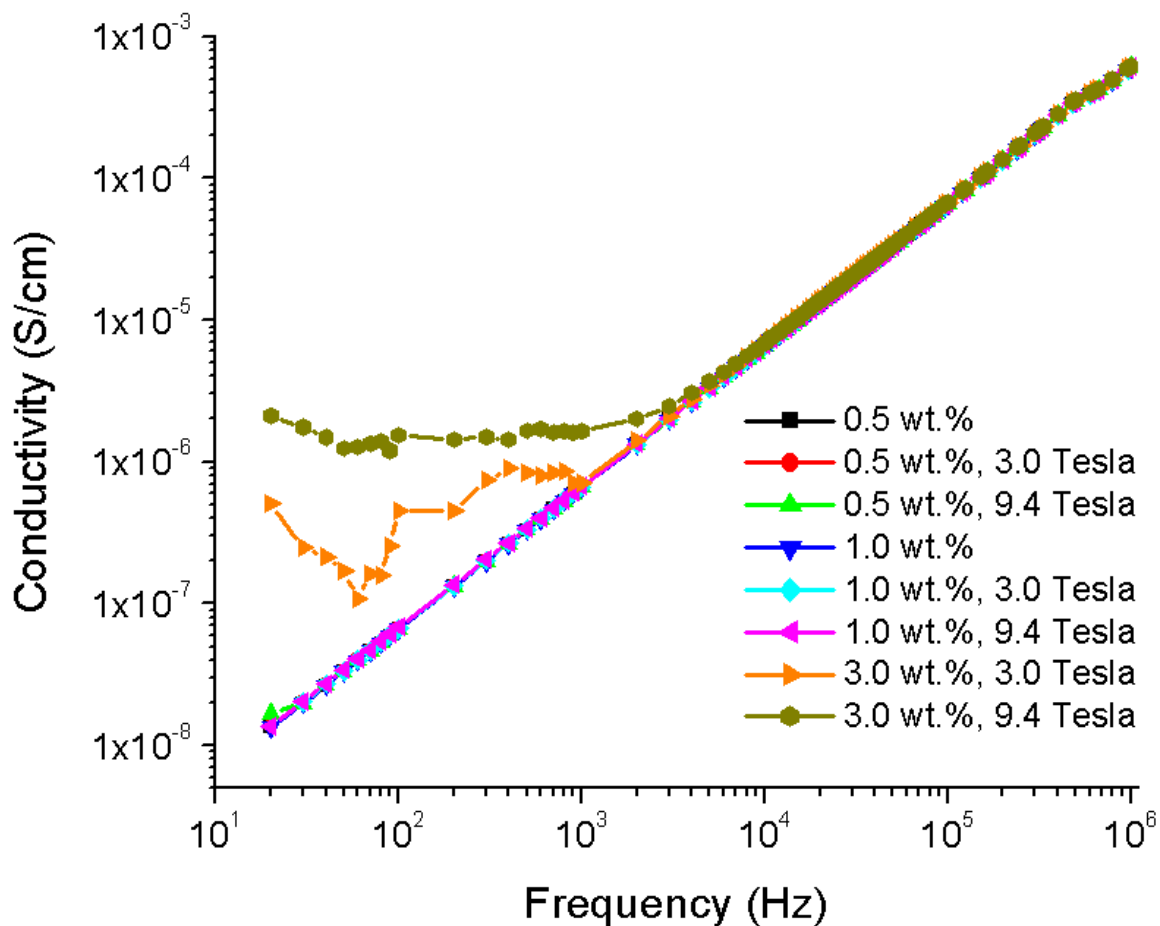


Figure 23. Log-log plot of the AC conductivity as a function of frequency for various nanocomposite samples.

The linear, frequency-dependent nature of the lower SWNT loading (0.5 and 1.0 wt.%) samples indicates dielectric behavior through an increase in the capacitive component of the impedance. By increasing the SWNT concentration to 3.0 wt.% more frequency-independent behavior is observed at relatively low frequency ranges (~20-2000 Hz), which is characteristic of a non-dielectric material. The non-dielectric range increases as the anisotropy of the SWNTs within the matrix increases, which suggests the magnetic field has an effect on the electrical behavior. To further understand the

electrical behavior of the nanocomposite samples, Figure 24 shows the conductivities at 60 Hz as a function of SWNT mass fraction and dependent upon magnetic field strength.

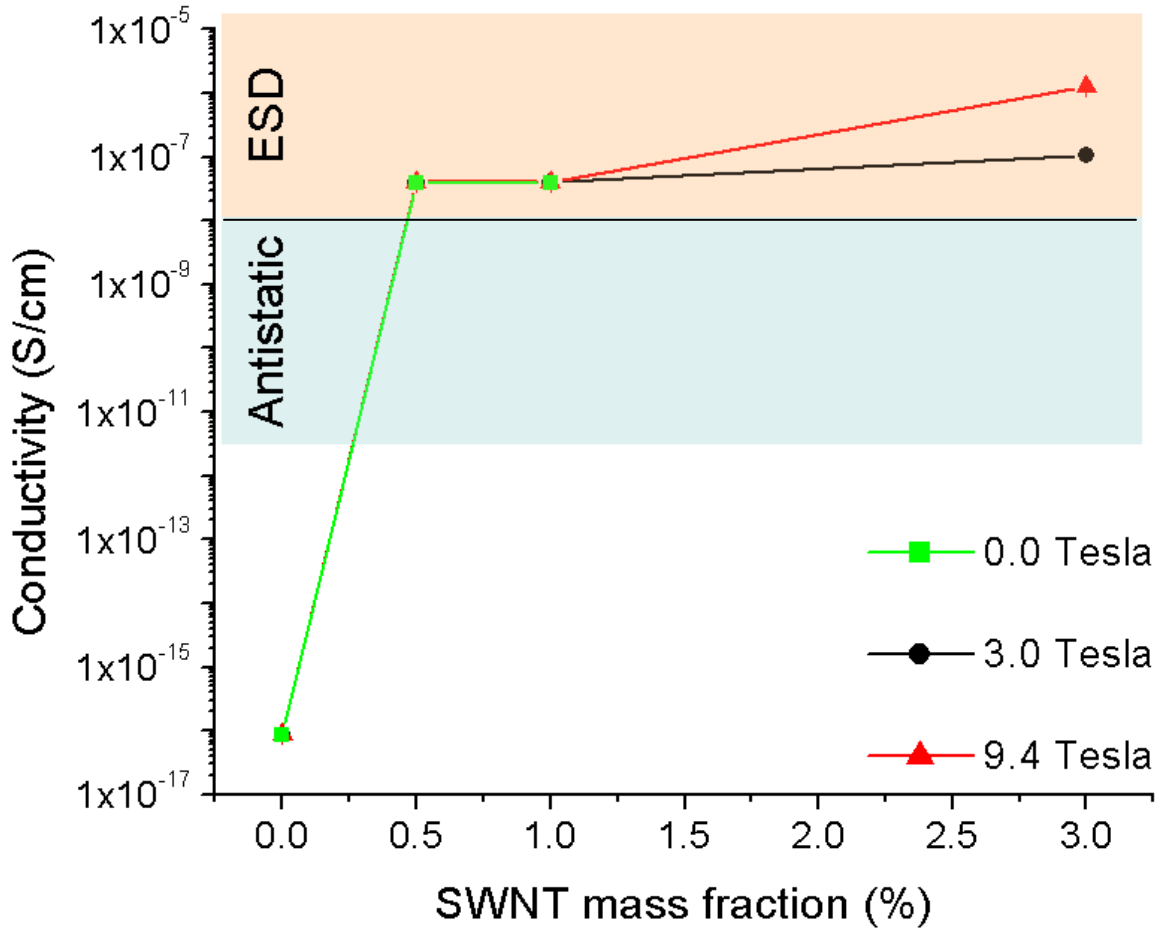


Figure 24. Log(AC conductivity) as a function of SWNT mass fraction showing dependence on magnetic field strength, and the relative applications based on the values.

By plotting conductivity as a function of SWNT concentration, the relative percolation threshold of each sample type can be estimated. Based on the conductivity of pure PET material, the addition of 0.5 and 1.0 wt.% SWNTs approximately produced a 7 order of magnitude increase, while the addition of 3.0 wt.% SWNTs in a 3 and 9.4 Tesla magnetic field produced an 8 and 9 order of magnitude increase, respectively. Therefore,

it can be safely assumed that the percolation threshold is approximately 0.5 wt.% SWNT. This value agrees satisfactorily with previous values observed in other polymer-CNT nanocomposite studies [54-56, 58, 61, 64, 65].

Also shown in Figure 23 are the relative applications for these materials based on their conductive behaviors. It is noticeable that at 0.5 wt.% SWNT, the conductivity of the samples exceeds the antistatic and electrostatic dissipation conditions, but EMI shielding ( $\sim 10^{-4}$  S/cm) would not be possible. Meeting the standards of the targeted applications is a very important goal of this work.

### *Analysis*

Analyzing the electrical measurements can improve the understanding of the relationship between processing, morphology, and properties of the nanocomposite material. The electrical properties are dependent upon the SWNT configuration within the PET matrix, which in turn is dependent upon the processing parameters. From the results, it is observed that when SWNT concentration reaches 3.0 wt.% there is an increase in electrical conductivity and non-dielectric behavior. The simple explanation to describe this behavior is to associate it with the increase in filler concentration and conclude that more filler material produces a more extensive electron flow network. However, a similar increase is not observed when the SWNT concentration reaches 0.5 and 1.0 wt.% for the unaligned or aligned samples, and so there must be supplementary details that require rationalization. Also, the explanation can not be directly connected to the creation of a percolation network at 3.0 wt.%, because as previously stated, a percolation threshold was achieved at no more than 0.5 wt.%.

To begin to form a conclusion about the electrical behavior, the frequency-dependent relationship of the samples must be interpreted (Figure 23). Frequency-dependence and dielectric behavior, such as that observed at 0.5 and 1.0 wt.%, is directly related to large gap distances between conductive particles within a matrix. Therefore, it implies that in the 0.5 and 1.0 wt.% samples the SWNTs flowed into aggregated domains during processing, increasing the distance between conductive particles, and resulting in relatively poor dispersion. This attraction between the SWNTs occurs because of van der Waals forces between the nanotubes [14, 15]. Though the electron flow may build up in the void space between the SWNT domains, within the insulating matrix material, the gap distances between domains are still not so great as to isolate the particles and completely retard any conductance. Current at very low frequencies (less than 20 Hz) is able to tunnel across the matrix and create a partial percolation network. Percolation is ideal, and conductivity is maximized, when physical contact exists between the CNTs, but it is not absolutely necessary to allow current to flow across a device [109].

When the SWNT concentration is 3.0 wt.% and manipulated with a magnetic field, there is a dramatic change in the electrical behavior at low frequencies. As mentioned, the change can not be attributed solely to filler concentration. This suggests that the magnetic fields must be invoking an effect. If the SWNTs have a tendency to aggregate, then something must be inhibiting this aggregation to some extent in the aligned 3.0 wt.% samples, because they display a frequency-independent, non-dielectric region at low frequencies (Figure 23). This behavior is more prominent (wider non-dielectric range, greater conductivity) for the 9.4 Tesla processed sample than for the 3 Tesla processed sample. The increased conductivity and non-dielectric range in the 9.4 Tesla sample

suggests that the sample has better dispersion. A more dispersed sample possesses smaller gaps between conductive particles, which means more electrons can easily ‘hop’ between particles and flow across a device.

How is this improved dispersion and greater electrical conductivity at higher concentrations of the aligned samples explained? It can not be solely due to improved alignment, because it has been concluded in a previous section that ideal alignment occurs at a low filler concentration and a high magnetic field strength. According to the Raman spectra (Figure 21), the 3.0 wt.% sample processed at 3 Tesla is basically isotropic with respect to the SWNTs. The 9.4 Tesla processed sample has slightly better alignment according to the respective spectra. Also, there is almost no difference in the electrical behavior between the aligned SWNTs processed at each magnetic field strength of the 0.5 and 1.0 wt.% samples. If the improved results had a direct correlation with alignment, then the same improvement observed at 3.0 wt.% should be observed at lower concentrations, especially since there is much greater disparity in the degree of alignment when comparing the effect of field strength at lower concentrations.

Therefore, if the explanation can not be attributed to concentration or alignment alone, then the answer may be a combination of these effects. The ability to flow into aggregated domains appears to be a problem for samples with lower concentration (0.5 and 1.0 wt.%), because there is plenty of void space between SWNTs, so as not to significantly inhibit their motion. This same effect was observed and discussed in the G-peak analysis of the Raman spectra to describe the alignment behavior. This may also help to explain the dispersion and conductivity improvement shown in the 3.0 wt.% samples. As shown in Figure 21, the SWNTs were not able to overcome the resistive

forces that arise with increased tube-to-tube interaction and solution viscosity, and thus align themselves within the matrix. If this interaction can inhibit motion in one plane, then why can it not have the same effect in all others? The 3.0 wt.% SWNT samples appear to exceed a ‘density threshold’, where the tendency to flow into aggregated domains is counteracted by the lack of void space and freedom to do so. Therefore, the SWNTs, for the most part, are forced to remain in a semi-dispersed state, which creates a better network and improved conductivity.

At the same time, the magnetic field is also producing a beneficial effect to the material. The 3.0 wt.% sample processed at 3 Tesla is essentially isotropic, and so the electrical improvement observed for this sample can be considered almost identical to the improvement that would be expected from a 3.0 wt.% sample not processed with an applied magnetic field. However, a 9.4 Tesla field is strong enough to invoke an effect, which could be explained with either of the following scenarios, or a combination of the two:

1. The magnetization, and force upon the nanotube, that a SWNT experiences from an applied magnetic field reduces the effect of the van der Waals forces that attract the SWNTs to each other. Thus, even though there is very little motion due to overcrowding of the SWNTs, any motion that does occur is halted and reduced further. This results in a more dispersed sample, and the increase in the non-dielectric range and conductivity observed in the results (Figures 23 and 24). A good method for testing this theory would be to process a low concentrated sample (~0.5 wt.% SWNT) while in the presence of a very high magnetic field strength (~20 Tesla) and measure the dispersion.

2. The slight improvement in alignment observed in Figure 21, when comparing the 3.0 wt.% sample processed at 3 Tesla to the 9.4 Tesla sample, creates a better and more anisotropic network, which improves electrical behavior. This same effect is not observed at lower concentrations (despite greater alignment), because the distance between the conductive particles is too great. Most likely, the effect of the magnetic fields is a combination of this scenario with the first scenario.

Overall, it appears that the most important contributing factors to electrical conductivity in a nanocomposite are filler concentration and dispersion. Alignment appears to impart a secondary consequence, as long as a 'density threshold' has been reached. An interesting finding seems to be that a strong enough magnetic field may improve dispersion by imparting axial motion, and thus inhibiting lateral motion. This could prove to be a very important attribute to consider for future nanocomposite manufacturing.

Dispersion has long been a key issue for creating effective nanocomposites with CNTs, because they have a high tendency to attract each other and aggregate, especially SWNTs [14, 15]. It has been shown that dispersion can be improved through modifying CNTs by adding functional groups to the ends and sides, which allows them to interact much more strongly with the surrounding matrix [31, 33, 75, 110-112]. However, modification also decreases the conductivity of individual CNTs by disrupting electron flow and reducing charge carriers along the axis [113-115]. This decrease in conductivity was offset by the notion that improved dispersion and percolation achieves an overall beneficial effect [109, 116]. It appears that at higher concentrations, and strong enough

magnetic fields, this issue may be easily resolved. Developing a method to achieve good dispersion of unmodified SWNTs in a polymer could produce unprecedented properties.

There are many questions that still remain. If a magnetic field can reduce aggregation, then how strong of a magnetic field would be required to achieve sufficient dispersion in a lower concentration sample where there is plenty of void space to allow SWNT motion? Would the utilization of such a magnetic field be more cost effective than modification through functionalization of the SWNTs? If not, could the property enhancement achieved by utilizing unmodified SWNTs be so great as to justify any additional cost?

Finally, even though there was less than perfect dispersion of the SWNTs, specifically at lower concentrations (0.5 and 1.0 wt.%), their inherent conductivity still managed to produce an electrically conductive nanocomposite film by solution casting. These electroconductive nanocomposites proved to be effective enough to fulfill requirements for antistatic and electrostatic dissipation applications.

## CHAPTER 6

### CONCLUSIONS

Solution casting was effectively employed to produce PET-SWNT nanocomposite films. SWNT morphology was investigated by Raman spectroscopy and TEM, and it was determined that the processing method did not negatively affect SWNT integrity. The crystallization behavior of the films was examined by DSC, and the SWNTs act as very effective nucleating agents that significantly enhance crystallization time and temperature. This has useful applications for large-scale manufacturing. Magnetic fields were employed to produce SWNT alignment within the PET matrix. Raman spectroscopy was used to measure the effectiveness of the magnetic fields, and it was determined that the field strength and filler concentration play the most important roles in determining the degree of alignment. Low concentration and high magnetic field strength produce the most highly aligned samples. The electrical properties of unaligned and aligned film samples were investigated by impedance spectroscopy, and it was shown that sufficient conductivity for antistatic and electrostatic dissipation purposes can be achieved at concentrations as low as 0.5 wt.% SWNT. It was also concluded that dispersion and filler concentration have the greatest effect upon electrical conductivity, and alignment plays a secondary role. However, it was determined that it may be possible to use a magnetic field to improve dispersion, or at least produce a more anisotropic network. This could have important implications in future applications, and it may prove to be a novel method for achieving good dispersion of unmodified SWNTs.

## LIST OF REFERENCES

1. Li S, Yu Z, Rutherglen C, Burke PJ. *Nano Lett.* 2004; 4:2003-2007.
2. Hamada N, Sawada S-i, Oshiyama A. *Phys. Rev. Lett.* 1992; 68:1579-1581.
3. Ebbesen TW, Lezec HJ, Hiura H, Bennett JW, Ghaemi HF, Thio T. *Nature* 1996; 382:54-56.
4. Langer L, Bayot V, Grivei E, Issi JP, Heremans JP, Olk CH, Stockman L, Van Haesendonck C, Bruynseraede Y. *Phys. Rev. Lett.* 1996; 76:479-482.
5. Tans SJ, Devoret MH, Dai H, Thess A, Smalley RE, Geerligs LJ, Dekker C. *Nature* 1997; 386:474-477.
6. Mintmire JW, Dunlap BI, White CT. *Phys. Rev. Lett.* 1992; 68:631-634.
7. Durkop T, Getty SA, Cobas E, Fuhrer MS. *Nano Lett.* 2004; 4:35-39.
8. White CT, Mintmire JW. *J. Phys. Chem. B* 2005; 109:52-65.
9. Zhou C, Kong J, Dai H. *Phys. Rev. Lett.* 2000; 84:5604.
10. *Conductive Polymers*. Business Communications Company, Inc. Norwalk, CT, 2003.
11. Colbert D. *Plastics, Additives & Compounding* 2003; 5:18-25.
12. Iijima S. *Nature* 1991; 354:56-58.
13. O'Connell MJ, editor. *Carbon Nanotubes: Properties and Applications*. Boca Raton, FL: CRC Press LLC; 2006.
14. Meyyappan M, editor. *Carbon Nanotubes: Science and applications*. Boca Raton, FL: CRC Press LLC; 2005.

15. Dresselhaus MS, Dresselhaus G, Avouris P, editors. Carbon Nanotubes: Synthesis, Structure, Properties, and Applications. New York, NY: Springer; 2001.
16. Dresselhaus MS, Dresselhaus G, Saito R. Carbon 1995; 33:883-891.
17. Dekker C. Physics Today 1999:22-28.
18. McEuen PL, Fuhrer MS, Hongkun P. Nanotechnology, IEEE Transactions on 2002; 1:78-85.
19. MatWeb. Automation Creations, Inc. 2007.
20. Primak W, Fuchs LH. Physical Review 1954; 95:22-31.
21. Rotkin SV, Subramoney S, editors. Applied Physics of Carbon Nanotubes: Fundamentals of Theory, Optics and Transport Devices. New York, NY: Springer; 2005.
22. Terrones M. Annu. Rev. Mater. Res. 2003; 33:419-501.
23. Lu JP. Phys. Rev. Lett. 1995; 74:1123-1126.
24. Likodimos V, Glenis S, Guskos N, Lin CL. Phys. Rev. B 2003; 68:045417.
25. Ajiki H, Ando T. Physica B: Condensed Matter 1994; 201:349-352.
26. Heremans J, Olk CH, Morelli DT. Phys. Rev. B 1994; 49:15122-15125.
27. Smith BW, Benes Z, Luzzi DE, Fischer JE, Walters DA, Casavant MJ, Schmidt J, Smalley RE. Appl. Phys. Lett. 2000; 77:663-665.
28. Walters DA, Casavant MJ, Qin XC, Huffman CB, Boul PJ, Ericson LM, Haroz EH, O'Connell MJ, Smith K, Colbert DT, Smalley RE. Chem. Phys. Lett. 2001; 338:14-20.
29. Ajiki H, Ando T. J. Phys. Soc. Jpn. 1995; 64:4382-4391.

30. Krishnamoorti R, Vaia RA, editors. Polymer Nanocomposites: Synthesis, Characterization, and Modeling. Washington D.C.: Oxford UP; 2002.
31. Andrews R, Weisenberger MC. *Curr. Opin. Solid State Mater. Sci.* 2004; 8:31-37.
32. Breuer O, Sundararaj U. *Polym. Compos.* 2004; 25:630-645.
33. Coleman JN, Khan U, Gun'ko YK. *Adv. Mater.* 2006; 18:689-706.
34. Sperling LH, *Introduction to Physical Polymer Science*. Hoboken, NJ: John Wiley & Sons, Inc.; 2006.
35. EPA. *Compilation of Air Pollutant Emission Factors, Volume I: Stationary Point and Area Sources*. 1991.
36. Zheng LX, O'Connell MJ, Doorn SK, Liao XZ, Zhao YH, Akhadov EA, Hoffbauer MA, Roop BJ, Jia QX, Dye RC, Peterson DE, Huang SM, Liu J, Zhu YT. *Nat Mater* 2004; 3:673-676.
37. Hummel RE, *Electronic Properties of Materials*. New York, NY: Springer; 2001.
38. Bhat NV, Joshi NV. *J. Appl. Polym. Sci.* 1993; 50:1423-1427.
39. Wu M, Shaw L. *J. Appl. Polym. Sci.* 2006; 99:477-488.
40. Cadek M, Coleman JN, Barron V, Hedicke K, Blau WJ. *Appl. Phys. Lett.* 2002; 81:5123-5125.
41. Safadi B, Andrews R, Grulke EA. *J. Appl. Polym. Sci.* 2002; 84:2660-2669.
42. Cadek M, Coleman J, Ryan K, Nicolosi V, Bister G, Fonseca A, Nagy J, Szostak K, Beguin F, Blau W. *Nano Lett.* 2004; 4:353-356.
43. Moniruzzaman M, Winey KI. *Macromolecules* 2006; 39:5194-5205.
44. Hone J, Whitney M, Piskoti C, Zettl A. *Phys. Rev. B* 1999; 59:R2514-R2516.
45. Che J, agin T, Iii WAG. *Nanotechnology* 2000; 11:65-69.

46. Berber S, Kwon Y-K, Tománek D. Phys. Rev. Lett. 2000; 84:4613-4616.
47. Fei D, Quan-Shui Z, Li-Feng W, Ce-Wen N. Appl. Phys. Lett. 2007; 90:021914-1 - 021914-3.
48. Hyperion, Catalysis, International. www.hyperioncatalysis.com.
49. Rutkofsky M, Folaron R. Zyvex's NanoSolve Technology: An Applications Overview. Zyvex Corporation. 2006.www.zyvex.com.
50. Jang J, *Conducting Polymer Nanomaterials and Their Applications*, in *Emissive Materials Nanomaterials*. 2006. p. 189-260.
51. Ajayan P, Stephan O, Colliex C, Trauth D. Science 1994; 265:1212-1214.
52. Ounaies Z, Park C, Wise KE, Siochi EJ, Harrison JS. Compos. Sci. Technol. 2003; 63:1637-1646.
53. Ogasawara T, Ishida Y, Ishikawa T, Yokota R. Composites Part A 2004; 35:67-74.
54. Hu G, Zhao C, Zhang S, Yang M, Wang Z. Polymer 2006; 47:480-488.
55. Anand KA, Agarwal US, Joseph R. J. Appl. Polym. Sci. 2007; 104:3090-3095.
56. Du F, Fischer JE, Winey KI. J. Polym. Sci., Part B: Polym. Phys. 2003; 41:3333-3338.
57. Andrews R, Jacques D, Minot M, Rantell T. Macromolecular Materials and Engineering 2002; 287:395-403.
58. Seo M-K, Park S-J. Chem. Phys. Lett. 2004; 395:44-48.
59. Kim YJ, Shin TS, Choi HD, Kwon JH, Chung Y-C, Yoon HG. Carbon 2005; 43:23-30.
60. Bumsuk K, Jongjin L, Insuk Y. J. Appl. Phys. 2003; 94:6724-6728.

61. Sandler JKW, Kirk JE, Kinloch IA, Shaffer MSP, Windle AH. *Polymer* 2003; 44:5893-5899.
62. McNally T, Potschke P, Halley P, Murphy M, Martin D, Bell SEJ, Brennan GP, Bein D, Lemoine P, Quinn JP. *Polymer* 2005; 46:8222-8232.
63. Zhang Q, Rastogi S, Chen D, Lippits D, Lemstra PJ. *Carbon* 2006; 44:778-785.
64. Chang TE, Kisliuk A, Rhodes SM, Brittain WJ, Sokolov AP. *Polymer* 2006; 47:7740-7746.
65. Antonucci V, Faiella G, Giordano M, Nicolais L, Pepe G. *Macromolecular Symposia* 2007; 247:172-181.
66. Shaffer MSP, Windle AH. *Adv. Mater.* 1999; 11:937-941.
67. Du F, Scogna RC, Zhou W, Brand S, Fischer JE, Winey KI. *Macromolecules* 2004; 37:9048-9055.
68. Tang H, Chen X, Tang A, Luo Y. *J. Appl. Polym. Sci.* 1996; 59:383-387.
69. Chen G-H, Wu D-J, Weng W-G, He B, Yan W-l. *Polym. Int.* 2001; 50:980-985.
70. Choi ES, Brooks JS, Eaton DL, Al-Haik MS, Hussaini MY, Garmestani H, Li D, Dahmen K. *J. Appl. Phys.* 2003; 94:6034-6039.
71. Watts P, Hsu W, Randall D, Kroto H, Walton D. *PCCP* 2002; 4:5655-5662.
72. Sennett M, Welsh E, Wright JB, Li WZ, Wen JG, Ren ZF. *Appl. Phys. A - Mater.* 2003; 76:111-113.
73. Jose MV, Steinert BW, Thomas V, Dean DR, Abdalla MA, Price G, Janowski GM. *Polymer* 2007; 48:1096-1104.
74. Lanticse LJ, Tanabe Y, Matsui K, Kaburagi Y, Suda K, Hoteida M, Endo M, Yasuda E. *Carbon* 2006; 44:3078-3086.

75. Abdalla M, Dean D, Adibempe D, Nyairo E, Robinson P, Thompson G. *Polymer* 2007; 48:5662-5670.
76. Ren ZF, Huang ZP, Xu JW, Wang JH, Bush P, Siegal MP, Provencio PN. *Science* 1998; 282:1105-1107.
77. Chris B, Wei Z, Sungho J, Otto Z. *Appl. Phys. Lett.* 2000; 77:830-832.
78. Huang ZP, Xu JW, Ren ZF, Wang JH, Siegal MP, Provencio PN. *Appl. Phys. Lett.* 1998; 73:3845-3847.
79. Park C, Wilkinson J, Banda S, Ounaies Z, Wise KE, Sauti G, Lillehei PT, Harrison JS. *J. Polym. Sci., Part B: Polym. Phys.* 2006; 44:1751-1762.
80. Martin CA, Sandler JKW, Windle AH, Schwarz MK, Bauhofer W, Schulte K, Shaffer MSP. *Polymer* 2005; 46:877-886.
81. Kimura T, Ago H, Tobita M, Ohshima S, Kyotani M, Yumura M. *Adv. Mater.* 2002; 14:1380-1383.
82. Garmestani H, Al-Haik MS, Dahmen K, Tannenbaum R, Li D, Sablin SS, Hussaini MY. *Adv. Mater.* 2003; 15:1918-1921.
83. Camponeschi E, Vance R, Al-Haik M, Garmestani H, Tannenbaum R. *Carbon* 2007; 45:2037-2046.
84. Correa-Duarte MA, Grzelczak M, Salgueirino-Maceira V, Giersig M, Liz-Marzan LM, Farle M, Sieradzki K, Diaz R. *J. Phys. Chem. B* 2005; 109:19060-19063.
85. Shi D, He P, Lian J, Chaud X, Bud'ko SL, Beaugnon E, Wang LM, Ewing RC, Tournier R. *J. Appl. Phys.* 2005; 97:064312.
86. Li Z, Luo G, Wei F, Huang Y. *Compos. Sci. Technol.* 2006; 66:1022-1029.
87. Anand KA, Agarwal US, Joseph R. *Polymer* 2006; 47:3976-3980.

88. Wang Y, Deng J, Wang K, Zhang Q, Fu Q. *J. Appl. Polym. Sci.* 2007; 104:3695-3701.
89. Shin DH, Yoon KH, Kwon OH, Min BG, Hwang CI. *J. Appl. Polym. Sci.* 2006; 99:900-904.
90. Probst O, Moore EM, Resasco DE, Grady BP. *Polymer* 2004; 45:4437-4443.
91. You J-W, Chiu H-J, Don T-M. *Polymer* 2003; 44:4355-4362.
92. Minus ML, Chae HG, Kumar S. *Polymer* 2006; 47:3705-3710.
93. Makela T, Jussila S, Kosonen H, Backlund TG, Sandberg HGO, Stubb H. *Synth. Met.* 2005; 153:285-288.
94. Shinohara H, Abe M, Nishi K, Arai Y. in *Photovoltaic Energy Conversion, 1994*. 1994.
95. Bachilo SM, Strano MS, Kittrell C, Hauge RH, Smalley RE, Weisman RB. *Science* 2002; 298:2361-2366.
96. Fernando KAS, Lin Y, Wang W, Cao L, Meziari MJ, Wang X, Veca ML, Zhang P, Quinn RA, Allard LF, Sun YP. *J. Phys. Chem. C* 2007; 111:10254-10259.
97. Chen G, Sumanasekera GU, Pradhan BK, Gupta R, Eklund PC, Bronikowski MJ, Smalley RE. *J. Nanosci. Nanotechnol.* 2002; 2:621-626.
98. Saito R, Takeya T, Kimura T, Dresselhaus G, Dresselhaus MS. *Phys. Rev. B* 1998; 57:4145-4153.
99. Yudasaka M, Zhang M, Jabs C, Iijima S. *Appl. Phys. A - Mater.* 2000; 71:449-451.
100. Hisao Y, Eriko S, Ayyakkannu M, Larry AN. *Appl. Phys. Lett.* 2001; 78:1355-1357.

101. Jabarin SA. J. Appl. Polym. Sci. 1987; 34:85-96.
102. Jabarin SA. J. Appl. Polym. Sci. 1987; 34:97-102.
103. Jabarin SA. J. Appl. Polym. Sci. 1987; 34:103-108.
104. Tong Sun JPRSP. J. Polym. Sci. Pol. Phys. 1984; 22:1163-1171.
105. Lu XF, Hay JN. Polymer 2001; 42:9423-9431.
106. Zhang Z, Ren M, Zhao J, Wu S, Sun H. Polymer 2003; 44:2547-2551.
107. Munson-McGee SH. Phys. Rev. B 1991; 43:3331.
108. Du F, Fischer JE, Winey KI. Physical Review B (Condensed Matter and Materials Physics) 2005; 72:121404.
109. Curran S, Zhang D, Wondmagegn W, Ellis A, Cech J, Roth S, Carroll D. J. Mater. Res. 2006; 21:1071-1077.
110. Lin Y, Zhou B, Shiral Fernando KA, Liu P, Allard LF, Sun YP. Macromolecules 2003; 36:7199-7204.
111. Eitan A, Jiang K, Dukes D, Andrews R, Schadler LS. Chem. Mater. 2003; 15:3198-3201.
112. Gojny FH, Nastalczyk J, Roslaniec Z, Schulte K. Chem. Phys. Lett. 2003; 370:820-824.
113. Dumitrescu I, Wilson NR, Macpherson JV. J. Phys. Chem. C 2007; 111:12944-12953.
114. Balasubramanian K, Burghard M. Small 2005; 1:180-192.
115. Kang C, Maeng IH, Oh SJ, Son J-H, Jeon T-I, An KH, Lim SC, Lee YH. in *International Topical Meeting on Microwave Photonics*. 2005.
116. Liu Y, Gao L. Carbon 2005; 43:47-52.